Structural Geological Model of the Kaunisvaara Mining District, Norrbotten, Sweden

Simon Husén

Dissertations in Geology at Lund University,
Master's thesis, no 677
(45 hp/ECTS credits)

Department of Geology
Lund University
2024

Structural Geological Model of the Kaunisvaara Mining District, Norrbotten, Sweden

Master's thesis

Simon Husén

Department of Geology
Lund University
2024

Table of contents

Cover Picture: Tapuli Central Pit, Kaunisvaara, Sweden (Simon Husén)

Structural Geological Model of the Kaunisvaara Mining District, Norrbotten, Sweden

SIMON HUSÉN

Husén, S., 2024: Structural Geological Model of the Kaunisvaara Mining District, Norrbotten, Sweden. *Dissertations in Geology at Lund University*, No 677. 47 pp. 45 hp (45 ECTS credits).

Abstract: The Kaunisvaara mining district, located in Norrbotten in northern Sweden, hosts several iron ore deposits, of which Tapuli and Sahavaara are the most economically important. The bedrock in the region has been subjected to several major deformation phases, which has created a complex structural pattern on a regional and local scale. Previous structural geological studies of the Tapuli deposit have mainly focused on a structural control on ore distribution and grade variations. This project, however, aims to provide a structural geological model of the mining area by emphasising brittle deformation. The main work was divided into two stages. The first stage included interpretations of pre-existing geophysical data (i.e., lineament analysis), aimed to outline the structural framework in a semi-regional perspective. The lineament analysis yielded 217 interpreted lineaments, showcasing at least two dominant structural trends, and indications of significant fluid flows in the Sahavaara deposit area. During the second stage, detailed structural measurements were collected by applying software-based operations to a point cloud-generated 3D model of the Tapuli mining pit. The approach, centred on digitizing and measuring fault planes, resulted in 137 structural measurements classified into three main orientations. The outcome of the respective analyses exhibited mostly consistent findings, reinforcing the observed dominant orientations across the geological formations and scales, and aligning well with previous studies. Indicated major fluid flows in the Sahavaara area remain inconclusive, emphasising the preliminary nature of interpretations based on geophysical data and highlighting the necessity of field verification for conclusive evidence. While proving to be a viable approach, the extraction of structural measurements from a point cloud-generated 3D model demonstrated inherent constraints when applied to brittle deformation in an open mining pit environment.

Keywords: structural geology, brittle deformation, lineament analysis, photogrammetry, point cloud

Supervisor: Professor Ulf Söderlund

Subject: Bedrock Geology

Strukturgeologisk modell över Kaunisvaara gruvområde, Norrbotten, Sverige

SIMON HUSÉN

Husén, S., 2024: Structural Geological Model of the Kaunisvaara Mining District, Norrbotten, Sweden. *Examensarbeten i geologi vid Lunds universitet,* Nr 677. 47 sid. 45 hp.

Sammanfattning: Kaunisvaara gruvområde, beläget i Norrbotten i norra Sverige, omfattar flera järnmalmsfyndigheter varav Tapuli och Sahavaara är de ekonomiskt mest betydande. Berggrunden i regionen har genomgått flera storskaliga deformationsfaser, vilket har skapat ett komplext strukturmönster på både regional och lokal skala. Tidigare strukturgeologiska studier av Tapulifyndigheten har främst fokuserat på den strukturella inverkan på malmfördelning och variationer i malmkvalitet. Detta projekt syftar i stället till att sammanställa en strukturgeologisk modell över gruvområdet genom att lägga tonvikt på spröd deformation. Det huvudsakliga arbetet delades upp i två delar. Den första delen innefattade tolkning av befintliga geofysiska data (dvs. lineamentsanalys) vilket syftade till att beskriva det strukturella ramverket ur ett semiregionalt perspektiv. Lineamentsanalysen, som resulterade i 217 tolkade lineament, uppvisar minst två dominerande strukturella trender samt indikationer på betydande vattenflöden i området runt Sahavaarafyndigheten. Under den andra delen samlades detaljerade strukturmätningar in från en punktmolnsgenererad 3D-modell över dagbrottet i Tapuli. Metoden, som involverade digitalisering och mätning av sprickplan, resulterade i 137 strukturmätningar vilka delades in i tre dominerande sprickgrupper. Utfallet från respektive metod visade i huvudsak på överensstämmande resultat, vilket styrker de observerade strukturella trenderna samt kongruerar väl med tidigare studier. Indikationer på storskaliga vattenflöden i Sahavaara förblir dock obekräftade, vilket understryker den preliminära karaktären av geofysiska tolkningar samt vikten av fältverifiering. Insamling av strukturmätningar från en punktmolnsgenererad 3D-modell fastställs som en gångbar metod som dock medför vissa begränsningar när den tillämpas på spröd deformation i dagbrottsmiljö.

Nyckelord: strukturgeologi, spröd deformation, lineamentsanalys, fotogrammetri, punktmoln

Handledare: Professor Ulf Söderlund

Ämnesinriktning: Berggrundsgeologi

1 Introduction

1.1 Background

The Kaunisvaara mining district is located in Norrbotten County, approximately 80 km north of the Arctic circle and 30 km north of the town of Pajala. The area hosts several iron ore deposits, of which Tapuli and Sahavaara are the most economically important (Figure 1). These deposits belong to an elongated cluster of iron-rich skarn mineralisation and banded iron formations (BIF) occurring over north-eastern Norrbotten from Masugnsbyn to the Pajala area. Additionally, several contiguous deposits, considered to be of similar type, have historically been mined in the Kolari district of Finnish Lapland to the east (e.g., Hannukainen and Rautuvaara). In Kaunisvaara, only the Tapuli deposit has been fully developed for mining, although the Sahavaara deposit has been extensively explored both historically and recently.

The Tapuli deposit is divided into two adjacent open pits (Central and North; Figure 2), each with distinct iron and sulphur grades. Mineralisation occurs as magnetite-rich skarn alteration associated with Karelian greenstones (c. 2.3–2.0 Ga) and Svecofennian sedimentary rocks (c. 2.0–1.8 Ga). Magnetite is the only ore mineral being mined and the total mineral resources (measured + indicated) amount to 90 Mt at a grade of 25.2% Fe and 0.4% S (Dishaw & Lepley, 2021). The extracted ore is processed into an iron concentrate (c. 68% Fe) on site and transported to the Norwegian port of Narvik for international shipping. KIAB's ambition is to expand the present mining operation to include the Sahavaara deposit, which already is covered by the current exploitation concession. Extensive exploration has recently been conducted in Sahavaara and potential mining of the deposit is subject to a pending environmental permit.

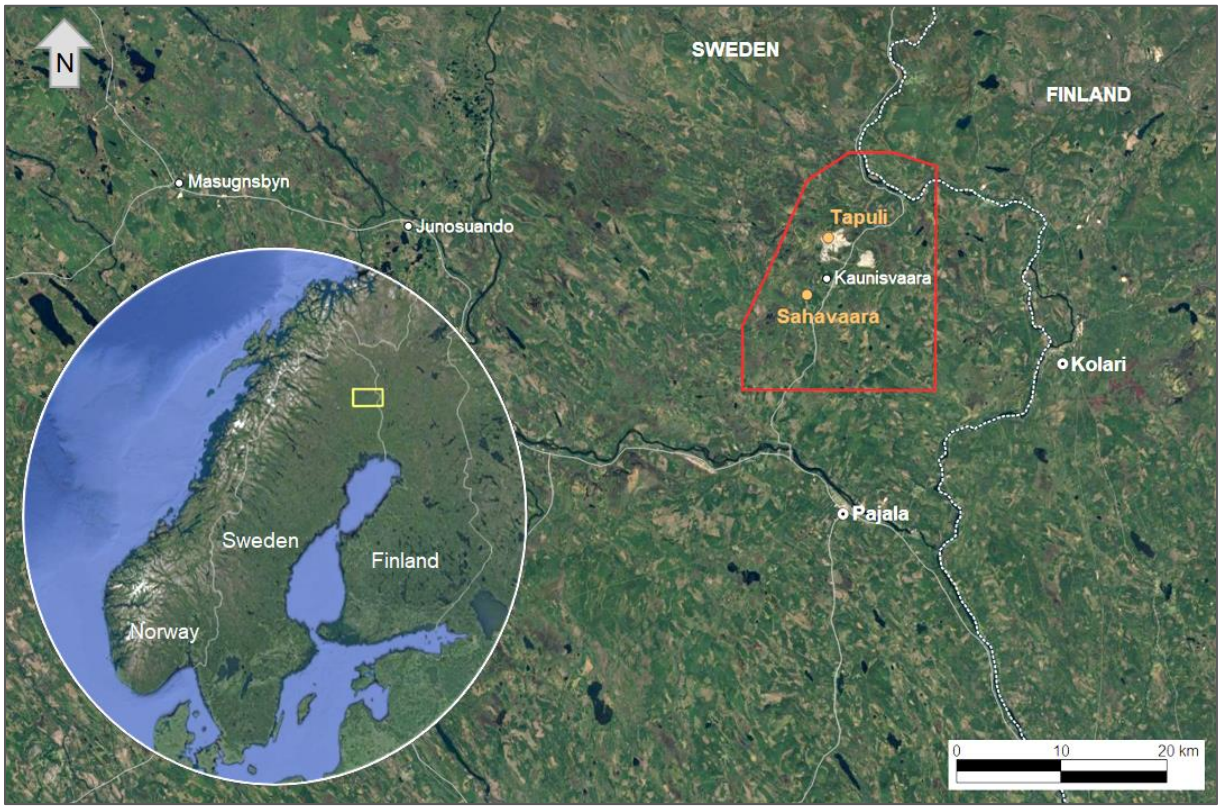

Figure 1. *Location of the two largest known iron ore deposits in the Kaunisvaara area: Tapuli and Sahavaara. The extent of the study area is indicated in red. Modified from Google Earth.*

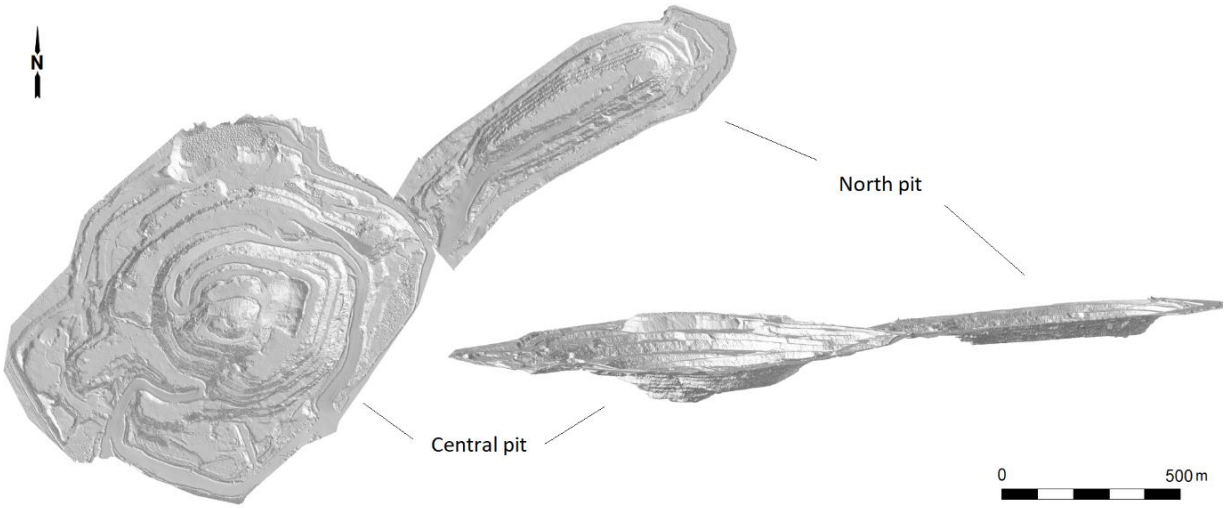

Figure 2. Current design of the Tapuli mine, divided into two adjacent open pits (Central and North). Left: view from above. Right: inclined view from the south.

In a structural geological context, the Tapuli and Sahavaara deposits are located on the western margin of the Pajala deformation belt (PDB); a major N-S striking shear zone that bisects the Fennoscandian shield from the Baltic Sea through northern Sweden, Finland, and Norway. The bedrock in the region has been subjected to several major deformation phases, primarily associated with the Svecokarelian orogeny (1.96–1.75 Ga), which has created a complex structural pattern on a regional and local scale.

Previous structural geological studies of the Tapuli deposit have mainly focused on the structural control on ore distribution and grade variations (e.g. Baker & Bonson, 2013). However, a general structural geological model of the mining area is lacking. Studying the local deformation patterns would provide insight into potential zones of mechanical weakness as well as structurally promoted ground water conduits, both of which are significant for the mining operation. Notably, groundwater leaking into drillholes is a recurring issue which occasionally leads to delays in the production. Structural geological information can therefore be incorporated in the short-term mine planning to mitigate the vulnerability of the production when mining in zones with challenging geological and hydrological conditions.

1.2 Scope of the thesis

This project aims to provide a structural geological model for the Tapuli mining area by interpreting pre-existing geophysical data alongside detailed structural measurements obtained during the project. The focus lies on brittle deformation, which poses more significant challenges to the daily mining operations compared to ductile analogues. The scope of this work encompasses the collection and utilization of geophysical interpretations and structural data to delineate the nature of extensive brittle deformation as well as locating and characterizing significant water-bearing fractures within the study area.

Furthermore, geological information regarding the Kaunisvaara deposits is dispersed across various studies and internal reports, complicating efforts to grasp the essence of these deposits. In tandem with its core objectives, this project seeks to consolidate and summarize prior studies on the Kaunisvaara deposits, particularly focusing on Tapuli, and to provide an overview of the geological context in which these deposits are situated.

2 Exploration and operational history

The Tapuli and Sahavaara deposits were discovered in 1918 by the geologist V. Tanner when conducting magnetic surveying in the Pajala area. Following the discovery, magnetic maps of the deposits were prepared and seven drillholes, totalling 464 m, were drilled in Tapuli (Lindroos et al., 1972). During the 1960s, the Swedish Geological Survey (SGU), with technical and financial aid from the mining consortium LKAB, carried out extensive iron ore exploration in Norrbotten (The Iron Ore Inventory Program). As part of the program, magnetic and gravity surveys were conducted in both Tapuli and Sahavaara. After the geophysical surveying was completed, 46 drillholes, totalling 11,798 m, were drilled in Sahavaara between 1961 and 1964 (Baker et al., 2011). Supplementary drilling during the 1970s extended the number of drillholes to 50 with a total length of 12,018 m. In Tapuli, the geophysical surveying was completed in 1965 and during the following four years 26 drillholes, totalling 6,280 m, were drilled in the deposit (Aker Solutions, 2010).

In the early 2000s, exploration in Kaunisvaara was resumed by Anglo American Exploration who carried out geophysical and geochemical surveying in the area. The geophysical surveys included magnetic ground measurements and electromagnetic ground and aerial surveys (Baker et al., 2011). In December 2004, Northland overtook the exploration license for the Tapuli and Sahavaara deposits. The following year, 14 drillholes, totalling 2,424 m, were drilled in Sahavaara; four of which were designated for metallurgic sampling (Aker Solutions, 2010). On commission from Northland, the Geological Survey of Finland (GTK) conducted aerial geophysical surveying in the Pajala area in August 2006. The survey included magnetic and electromagnetic measurements, as well as gamma ray spectrometry. In 2007, Northland drilled the Tapuli deposit with the purpose to update existing drill data and collect fresh metallurgic samples. The campaign resulted in 37 drillholes for a total of 5,695 m. Subsequently, an additional 69 drillholes, totalling 13,184 m, were drilled in Tapuli between September 2007 and April 2008. A substantial portion of the additional cores were collected from the central deposit to be used for pilot plant testing (Aker Solutions, 2010).

In November 2008, Northland was granted exploitation concession for the Tapuli deposit. The following year, geotechnical and hydrological drilling were carried out in Tapuli by Vattenfall AB and Pöyry Environment Oy (Pöyry), respectively. The drilling resulted in seven geotechnical drillholes, totalling 2,480 m, and 11 hydrological drillholes, totalling 3,091 m (Perman et al., 2009; Saksa et al., 2009). Following allowance of the environmental permit in August 2010, mining commenced at Tapuli in November 2012. Mining continued until October 2014 when Northland filed for bankruptcy due to falling market prices and all mining was terminated. The Northland bankruptcy estate was acquired by KIAB in February 2018 and mining in Tapuli was resumed in July the same year. In 2019, KIAB reached full production, equivalent of two million tonnes of iron concentrate per year.

Recent drilling of the Sahavaara deposit was completed in May 2021, including 80 metallurgic and nine exploration drillholes, totalling 10,611 m. A total of 22 tonnes of ore, collected from the metallurgic cores, were used for pilot plant testing in which floatation processing was applied. Sulphur concentrations were reduced below 0.05% S in the final test product, which can be correlated to a typical market requirement of ≤0.07% S. A summary of all conducted drilling in the Tapuli and Sahavaara deposits, both historical and recent, is presented in Table 1.

Table 1. Summary of all exploration, metallurgic, geotechnical, and hydrological drilling of the Tapuli and Sahavaara deposits until October 2021.

Deposit	Number of drillholes	Drilling (m)
Tapuli	157	31,194
Sahavaara	153	25,053
Total	**310**	**56,247**

3 Regional geology

3.1 Lithostratigraphy in northern Norrbotten

The northern region of the Fennoscandian shield (Figure 3), including parts of Sweden, Finland, and Norway, is one of the most economically important metallogenic provinces in Europe, dominated by a variety of iron oxide and Cu±Au deposits. Unlike many other shield domains, the Fennoscandian shield was primarily mineralised during the Paleoproterozoic rather than the Archean (Martinsson et al., 2016). The Paleoproterozoic bedrock in northern Norrbotten formed during the Svecokarelian orogeny (1.96–1.75 Ga) and includes older Archean and Paleoproterozoic rocks, as well as younger syn-orogenic rocks. Svecokarelian intrusions, Svecofennian supracrustal rocks, and pre-existing Karelian and Archean rocks make up the majority of the orogen, most of which were metamorphosed and deformed to varying extent during orogenic progresses.

3.1.1 Archean rocks (>2.5 Ga)

The Archean rocks occur in a limited extent in the northernmost part of Norrbotten and few studies of them have been made. These rocks mainly belong to the so-called Råstojaure complex and are comprised of gneissic granitoids with granodioritic to tonalitic composition (Bergman, 2018). The granitoids presumably crystallized at 2.8–2.7 Ga and were subsequently subjected to regional metamorphism around 2.7 Ga (Martinsson et al., 1999). Locally, banded paragneisses occur, which likely constitute the pre-existing supracrustal rocks into which the granitoids intruded (Bergman et al., 2001). Heavily deformed mafic to ultramafic intrusive rocks with an age of roughly 2.5–2.4 Ga occurs in the Archean basement and are believed to correlate with the initial stages of continental rifting during the early Proterozoic (Lahtinen et al., 2015; Martinsson, 1997).

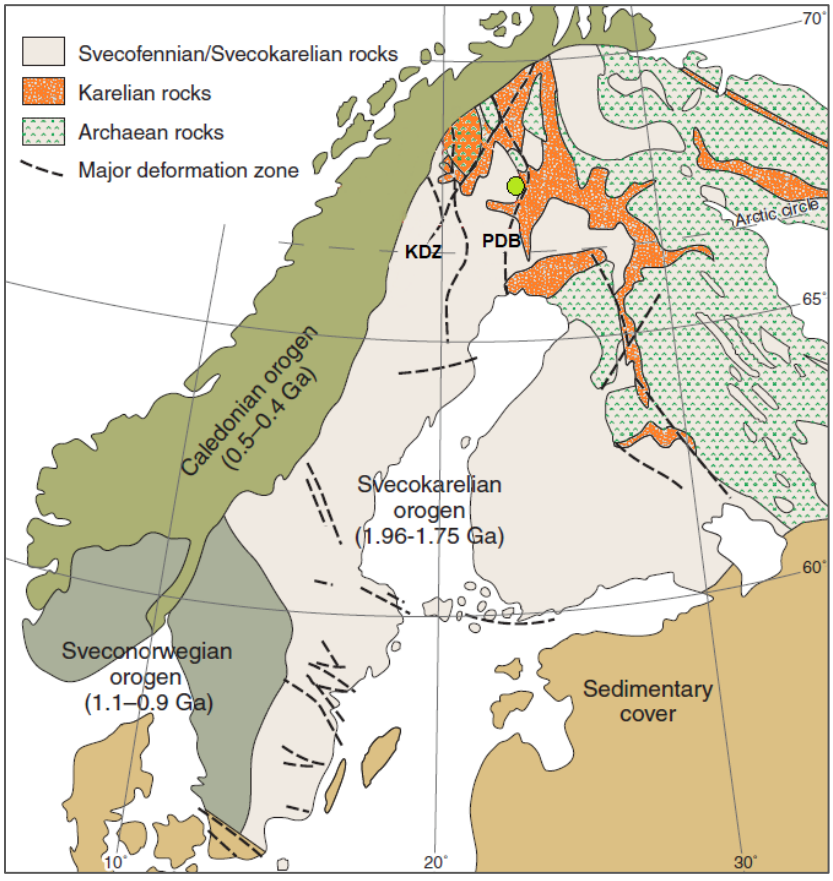

Figure 3. The major geological units in the Fennoscandian Shield and surrounding areas. Location of the Kaunisvaara mining district is indicated by the green dot. PDB = Pajala deformation belt. KDZ = Karesuando-Arjeplog deformation zone. Modified from Bergman et al. (2001).

3.1.2 Karelian rocks (c. 2.5–2.0 Ga)

The Archean rocks are discordantly overlain by a Paleoproterozoic supracrustal sequence comprised of Karelian metasedimentary and metavolcanic rocks (Bergman, 2018). The lowermost unit of the Karelian sequence, the so-called Kovo group (Figure 4), is comprised of clastic metasedimentary rocks, primarily conglomerate and quartzite, deposited along the shoreline of an expanding rift zone (Martinsson, 1997; Bergman et al., 2001). The clastic rocks are overlain by tholeiitic metabasalts and calc-alkaline metavolcanic rocks of andesitic composition, constituting the uppermost portion of the Kovo group (Bergman, 2018). North of Kiruna, a diabase intruding the lower clastic formation has been dated to approximately 2.2 Ga, hence giving the minimum depositional age of the Kovo group (Bergman et al., 2001).

The upper part of the Karelian sequence is comprised of chlorite- and serpentine-altered mafic to ultramafic metavolcanics, as well as minor carbonate and clastic metasedimentary rocks. In the Kiruna area, these rocks are included in the Kiruna greenstone group (Figure 4) and are associated with the Cu deposit Viscaria (Martinsson, 2004; Bergman, 2018). In the area between Kiruna and Pajala, the stratigraphic arrangement is comparable, but not equally complete, and occurs as the Veikkavaara greenstone group (Bergman, 2018). The latter host numerous iron deposits in the form of banded iron formations and skarn mineralisation commonly associated with carbonates and graphitic schists or phyllites (Martinsson et al., 2018; Lynch et al., 2018b). Massive units of crystalline carbonate rocks are found at high stratigraphic levels within the greenstone group in the Vittangi, Masugnsbyn and Pajala areas. Accordingly, a <200 m thick unit of dolomite forms the footwall to the Tapuli iron skarn mineralisation (Bergman et al., 2001). Deposition of the greenstone group is suggested to have taken place during a phase of intensive rifting sometime before 2.14 Ga (Martinsson, 1997; Bergman, 2018).

3.1.3 Svecofennian rocks (c. 2.0–1.75 Ga)

Svecofennian supracrustal rocks overlie parts of the greenstone group and mark the onset of the Svecokarelian orogeny. The lowermost portion of this formation is dominated by calc-alkaline metavolcanic rocks with basaltic to andesitic composition, interbedded with siliciclastic metasediments (Bergman, 2018). These rocks belong to the Porphyrite group (Figure 4) and presumably formed in a subduction-related compressional environment on the margin of the Archean craton (Martinsson & Perdahl, 1995). East of Kiruna, stratigraphically equivalent rocks, formed from contemporaneous andesitic volcanism, are commonly referred to as the Sammakkovaara group (Martinsson et al., 2016).

The overlying Porphyry group (Figure 4), which consists of metamorphosed basalts, andesites, dacites, and rhyolites, hosts the economically important apatite-iron ores in the Kiruna area (Bergman et al., 2001). Metamorphosed andesitic lava beds form the footwall to the extensive Kiirunavaara mineralisation, while the hanging wall is comprised of a porphyritic metadacite (Bergman, 2018; Martinsson, 2004). Dating of the Kiruna ores suggests mineralisation ages around 1.88–1.87 Ga and the age of the host rocks have been constrained at 1.89–1.88 Ga (Westhues et al., 2016). Deposition of the Porphyry group marks a shift from the calc-alkaline compositions, associated with the underlying Porphyrite group, to more alkaline magmatism (Bergman et al., 2001). Additionally, a clastic sequence comprised of primarily meta-arenites, with minor metamorphosed conglomerate and mudstone, constitute the youngest Svecofennian supracrustal rocks. The conglomerate locally enfolds a metadiorite with an age determined at 1.88 Ga, thus marking the maximum age of the clastic deposition (Bergman, 2018).

Several generations of intrusive rocks occur in the Svecofennian sequence. The so-called Perthite monzonite suite (1.88–1.86 Ga; Figure 4) is found mainly in north-western Norrbotten and is comprised of predominantly quartz-poor intrusive rocks such as monzonite and quartz monzonite, but also granite (Bergman, 2018). Several voluminous intrusions of gabbro and diorite are commonly associated with

the suite. Further east, the Haparanda suite (1.89–1.88 Ga; Figure 4) is comprised of a similar spectrum of intrusive rocks, ranging from gabbro to monzonite and granite, but have traditionally been set apart due to a distinctive geochemical signature. Rocks of the Haparanda suite are typically calc-alkaline in composition, whereas the Perthite-monzonite suite is more alkaline (Bergman, 2018). A series of S-type granites and granitoids with an approximate age of 1.85 Ga occur over a widespread area to the northeast and have been referred to as the Jyryjoki granite (Hellström & Bergman, 2016; Martinsson et al., 2016). Massive intrusive rocks, belonging to the Lina suite (1.81–1.76 Ga), occur on a regional scale in northern Norrbotten and are comprised of fine grained, foliated S-type granites associated with pegmatites and granitic dykes (Bergman, 2018; Martinsson et al., 2016).

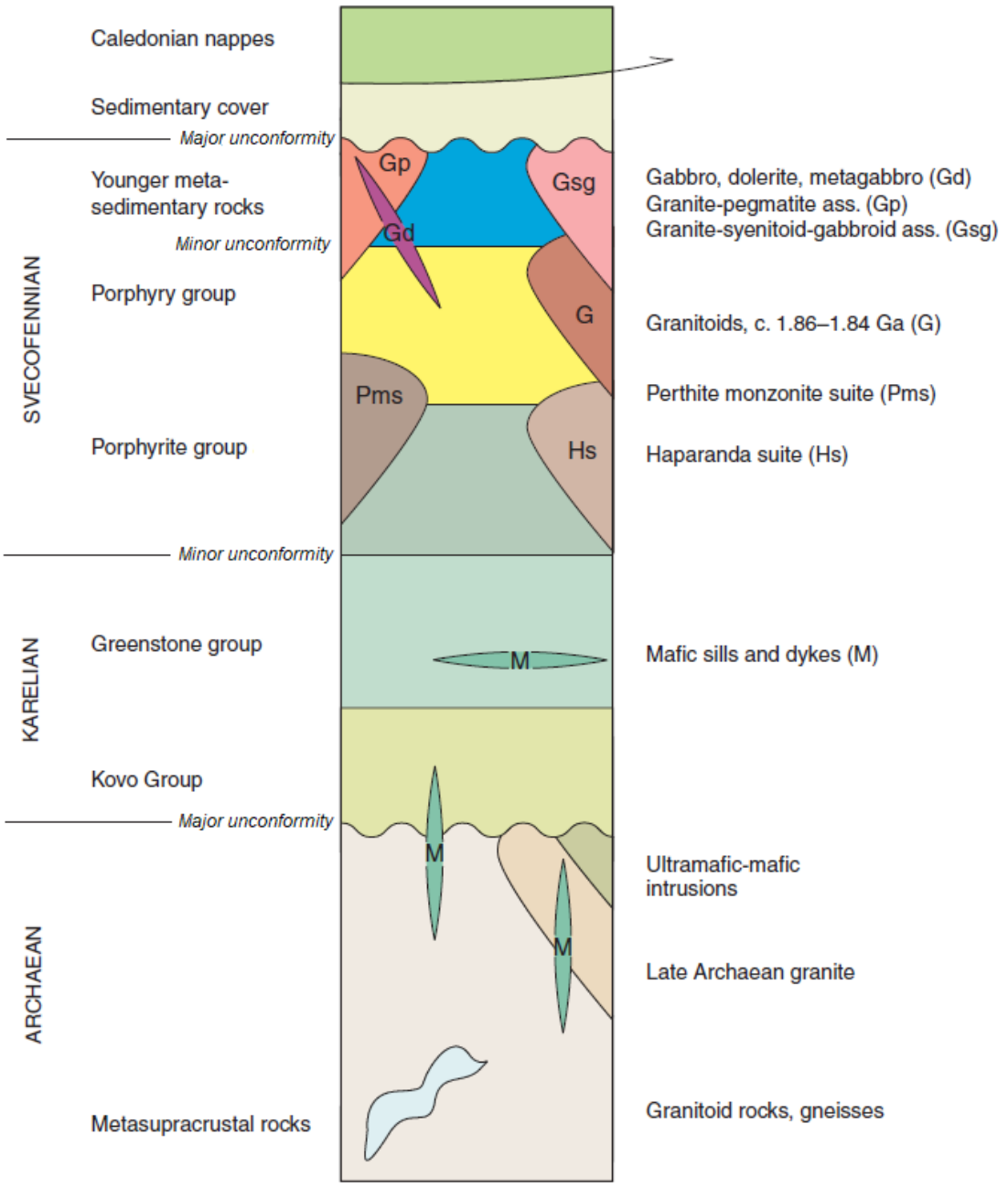

Figure 4. Schematic diagram of the northern Norrbotten stratigraphy with major rock units shown (not to scale). Modified from Bergman et al. (2001).

3.2 Regional deformation and tectonics

Northern Norrbotten has been subjected to several phases of brittle and ductile deformation spanning from the Archean to more recent times (including late- to postglacial faulting). Regional ductile deformation is primarily associated with the Svecokarelian orogeny and includes extensive folding and development of large-scale shear zones, such as the Pajala deformation belt (PDB) and Karesuando-Arjeplog deformation zone (KDZ; Figure 3). The metamorphic grade varies regionally but generally increase eastwards, from lower greenschist facies to upper amphibolite facies. Locally, the metamorphic grade reaches granulite facies in the easternmost part of Norrbotten (e.g., the Pajala area), while the lowest metamorphic grade is found in the Kiruna and Stora Sjöfallet areas to the west (Luth et al., 2018; Bergman et al., 2001).

The extent of deformation ranges from weakly developed foliation to heavily deformed migmatites, and major fold structures can be found in the majority of the supracrustal rocks in the region (Bergman et al., 2001). Conformant with the metamorphic grade, intensity and complexity of the deformation also increase eastwards. Consequently, the Kiruna area appears to only have undergone one major phase of ductile deformation (Luth et al., 2018), although Wright (1988) suggested multiple minor deformation events in the area. Further east, the structural pattern is more complex and includes several major ductile deformation phases (Grigull et al., 2018; Luth et al., 2018). In the Vittangi area, for instance, two separate trends of folding have been identified in the greenstone group, where weakly developed NW-SE oriented folds occur together with more pronounced N-S oriented folds (Bergman et al., 2001). These two structural orientations constitute the dominant ductile trends in the region, particularly in the eastern parts where polyphase deformation is more evident. In addition, a third distinct structural trend, expressed as NE-SW oriented folding, have been identified within the PDB in the Pajala area (Luth et al., 2018).

Brittle deformation is manifested as several distinct groups of deeply rooted faults, with both dextral and sinistral kinematics, occurring on a regional scale (Bergman et al., 2001). Phases of crustal faulting ranges from brittle-ductile deformation events during the mid to late Svecokarelian, to purely brittle phases in postglacial times.

3.2.1 Archean deformation

Bergman et al. (2001) observed that the structural trends are similar in the Archean and Paleoproterozoic rocks in the region. In previous studies, it has therefore been difficult to determine if structures in Archean rocks are a result of Svecokarelian reworking, or if these structures existed prior to the orogenic event. Nevertheless, granitic clasts in a conglomerate north of Kiruna, belonging to the Kovo group, shows random foliation directions, indicating that deformation predates the deposition and therefore occurred prior to the Svecokarelian orogeny (Bergman et al., 2001). Deformation and metamorphism during the Archean are poorly constrained, but Bergman et al. (2001) suggested that the youngest deformation event of Archean rocks occurred sometime after 2.7 Ga. This is consistent with the 2.7 Ga metamorphic event reported by Martinsson et al. (1999) and may correlate with the N-S oriented foliation direction observed in Archean rocks in northernmost Norrbotten.

3.2.2 Svecokarelian deformation

The Svecokarelian orogeny covered at least two major phases of deformation and metamorphism. The first phase included reworking of Archean structures and deformation of pre- and syn-orogenic Paleoproterozoic rocks, followed by a major change in magmatism and deformation intensity (Bergman et al., 2001). In a short amount of time, the melts shifted from calc-alkaline (e.g., Porphyrite group and Haparanda suite) to more alkaline compositions (e.g., Porphyry group and Perthite-monzonite suite).

The shift in magma composition has been suggested to correlate with the transition from a subduction-dominated to an extensional tectonic setting (Martinsson & Perdahl, 1995). In north-western Norrbotten, intrusive rocks of the Perthite-monzonite suite (1.88–1.86 Ga) forms N-S oriented belts, which may indicate an E-W extensional direction at the time. Additionally, Bergman et al. (2001) proposed that the transition was accompanied by an abrupt break of regional ductile deformation and metamorphism around 1.88 Ga.

Lahtinen et al. (2015) presented a slightly different tectonic model for the region. These authors suggested that continental rifting occurred at 2.1–2.05 Ga, followed by subduction and development of a magmatic arc around 2.0 Ga. Ultimately, continent-continent collision occurred at 1.92–1.91 Ga. The extensional environment, inferred by Martinsson & Perdahl (1995), may correspond with a subduction-related extensional setting (e.g., back-arc basin), although the timing is inconsistent with Lahtinen et al. (2015). Nonetheless, U-Pb dating of zircons found in migmatitic rocks in the Masugnsbyn area indicates a single phase of deformation and metamorphism around 1.88 Ga (Hellström, 2018). This is coherent with older studies of the iron deposits in Kirunavaara and Sautusvaara (25 km east of Kiruna), suggesting a phase of deformation and folding around 1.88 Ga (Romer et al., 1994; Eriksson & Hallgren, 1975).

The second major deformation phase related to the Svecokarelian orogeny occurred around 1.86–1.77 Ga (Bergman et al., 2001) and was primarily concentrated along large-scale deformation zones, such as the PDB and KDZ. Local observations and interpretations of magnetic data in previous studies indicate that deformation occurred in a dextral transpressive tectonic regime associated with NE-SW to E-W compression (Bergman et al., 2001). Major fold structures likely already existed but were reworked and attained their current geometry during this time. Areas with the highest metamorphic grade were confined to north-eastern Norrbotten and associated with the major deformation zones (Luth et al., 2018). Dating of a monzonite in Masugnsbyn indicate a metamorphic event constrained at 1.86–1.85 Ga (Bergman et al., 2006). Furthermore, several consecutive deformation phases, corresponding with the waning stage of the orogenic evolution, occurred between 1.83 Ga and 1.77 Ga and generated the youngest ductile deformation in the region (Bergman et al., 2001; Lahtinen et al., 2015; Hellström & Bergman, 2016). This late stage included dextral transpressive kinematics, accommodating ductile and brittle-ductile deformation along the PDB and KDZ. U-Pb dating of migmatites south of Pajala yield metamorphic ages between 1.81 and 1.77 Ga, which implies that the PDB was active during this time (Bergman et al., 2001). Local hydrothermal alteration and formation of ore deposits were likely promoted by the tectonic and magmatic activity during mid to late stages of the Svecokarelian orogeny.

3.2.3 Brittle deformation

Brittle deformation is poorly exposed in the region and has primarily been interpreted from geophysical data in previous studies. Three major groups of discontinuities, oriented NW-SE, NNW-SSE and NNE-SWW have been identified from magnetic and gravity datasets (Luth et al., 2018; Bergman et al., 2001). All three groups occur on a regional scale and can be traced several km into the crust. Bergman et al. (2001) approximated that more than 10% of the magnetic lineaments display signs of dextral movement, preferentially in the group with NW-SE orientation. Roughly 5% show signs of sinistral movement and were, almost exclusively, found in lineaments with NE-SW orientation. The perpendicular relationship between these two sets indicates that faulting occurred in response to N-S directed compression. Consequently, the brittle kinematic pattern deviates from the regional ductile analogue, which is manifested as extensive NW-SE to N-S orientated folding. The timing of brittle deformation in the region is generally poorly constrained, but U-Pb dating of monazite and titanite crystals in a fault zone in Malmberget indicates ages of 1.74 Ga and 1.62 Ga, respectively (Romer, 1996). Additionally, large portions of the PDB and KDZ are believed to have been reactivated under brittle to brittle-ductile conditions after the major ductile deformation phases (Bergman et al., 2001).

3.3 Pajala deformation belt (PDB)

As shown in Figure 3, the Tapuli and Sahavaara deposits are located on the western margin of the PDB. Berthelsen & Marker (1986) originally named the PDB the Baltic-Bothnian mega shear and interpreted the deformation as the result of extensive intraplate strike-slip movement. Kärki et al. (1993) later added a dextral kinematic component and renamed the belt the Pajala shear zone. Subsequently, tectonic models have been presented by Nironen (1997), who proposed that the PDB is a result of continental rifting, and Lahtinen et al. (2015), who suggested that deformation occurred in response to reactivation of an ancient suture zone. Both models include multiple deformation phases with both dextral and sinistral movement.

Structural geological studies along the Swedish part of the PDB have historically been scarce, and the tectonic interpretations above are based primarily on aerial geophysical patterns and geochronological data collected from major tectonic units in the area. However, a more recent study by Luth et al. (2018), focusing on the Swedish part of the PDB, outlines the characteristics and deformational history by integrating structural mapping with interpretations of geophysical data and 3D modelling. Most of the information used to summarize the tectonic history of the PDB in the following sections is based on Luth et al. (2018) and Lahtinen et al. (2015).

3.3.1 Structural framework

South of Pajala, the PDB is composed of numerous parallel and intersecting shear zones, striking mainly N-S, with a combined width of roughly 60 km. The boundary of the PDB is delimited in the west by the steeply east-dipping Koijuvaara shear zone, and steeply west-dipping shear zones in the east (Luth et al., 2018). To the north, the belt bends eastward into Finland where it is intersected by the NE-SW striking Kolari shear zone (KSZ; Figure 5). Seismic profiles and mapping across the Finnish part of the PDB and KSZ have previously uncovered several shear zones with variable orientations, indicating multiple phases of deformation (Niiranen, 2011). Polyphase deformation is further reflected in the complex structural pattern in the region, manifested by different generations of superimposed and interfering folds. Grigull et al. (2018) proposed that major NW-SE oriented folds (F1) were subsequently refolded by a younger generation of N-S trending folds (F2). This is consistent with the tectonic model by Luth et al. (2018), which includes three major deformation phases: D1, D2 and D3 (Figure 5). Here, the PDB is interpreted to have formed during an initial stage of NE-SW dextral transpressive shortening (D1), creating a transpressional wedge between the eastern and western bounding shear zones. D1 was followed by a phase of E-W directed shortening (D2), during which the KSZ developed. Faulting and sinistral brittle-ductile reactivation of the PDB was accommodated by a final phase of NNW-SSE shortening (D3).

The NW-SE oriented folding pattern of F1 is coherent with the shortening direction during D1. Likewise, the subsequent refolding by the N-S oriented folds (F2) is consistent with the shortening direction of D2. Structural reworking by F2 was primarily concentrated along N-S striking shear zones within the PDB. Luth et al. (2018) suggested that some of the inferred refolding may be a result of rotation due to non-coaxial strain within the deformation belt. In addition, the same authors outlined several NE-SW oriented folds occurring along a NE striking belt which intersects the northern part of the PDB. This belt is interpreted as the southwestern extension of the KSZ and the NE-SW oriented structures within clearly deviate from F1 and F2.

The PDB and KSZ overlap large parts of the Kaunisvaara and Kolari ore districts, and a structural control on the formation of the metallogenic area is indicated by studies on the Finnish deposits (Niiranen et al., 2007). In Tapuli, a deposit-scale isoclinal anticline-syncline pair in the central part of the deposit have been identified by modelling of the mineralisation-footwall contact (see Baker & Bonson, 2013). The NE-SW orientation of the Tapuli folds is consistent with the structural trends within the PDB-KSZ

intersection and may have formed concurrently with F2 as the KSZ developed during D2 (Figure 5). Baker & Bonson (2013) interpreted the folding in Tapuli to correlate with dextral transpression along a NE trending shear zone, referred to as the Tapuli shear zone.

3.3.2 Metamorphism and age constraints

Ductile deformation along the PDB occurred under medium to high-grade metamorphic conditions promoted by the Svecokarelian orogeny (Curtis et al., 2018). Lahtinen et al. (2015) reported at least three metamorphic events in the region, constrained at 1.92–1.90 Ga, 1.85 Ga, and 1.82–1.78 Ga. The latter event being consistent with the 1.81–1.77 Ga migmatites south of Pajala reported by Bergman et al. (2001). The youngest event is either a single continuous event at 1.82–1.78 Ga or, alternately, two events at 1.83–1.82 Ga and 1.79–1.77 Ga, respectively (Lahtinen et al., 2015). Still, pegmatitic granites with ages of around 1.79–1.77 Ga occur in high-grade areas and seem to correspond with a final major thermal event before crustal stabilization. Moreover, Luth et al. (2018) suggested that deformation during D2 occurred no earlier than 1.8 Ga, based on the young metamorphic ages (1.8 Ga) within the PDB compared with its surroundings (1.84 Ga).

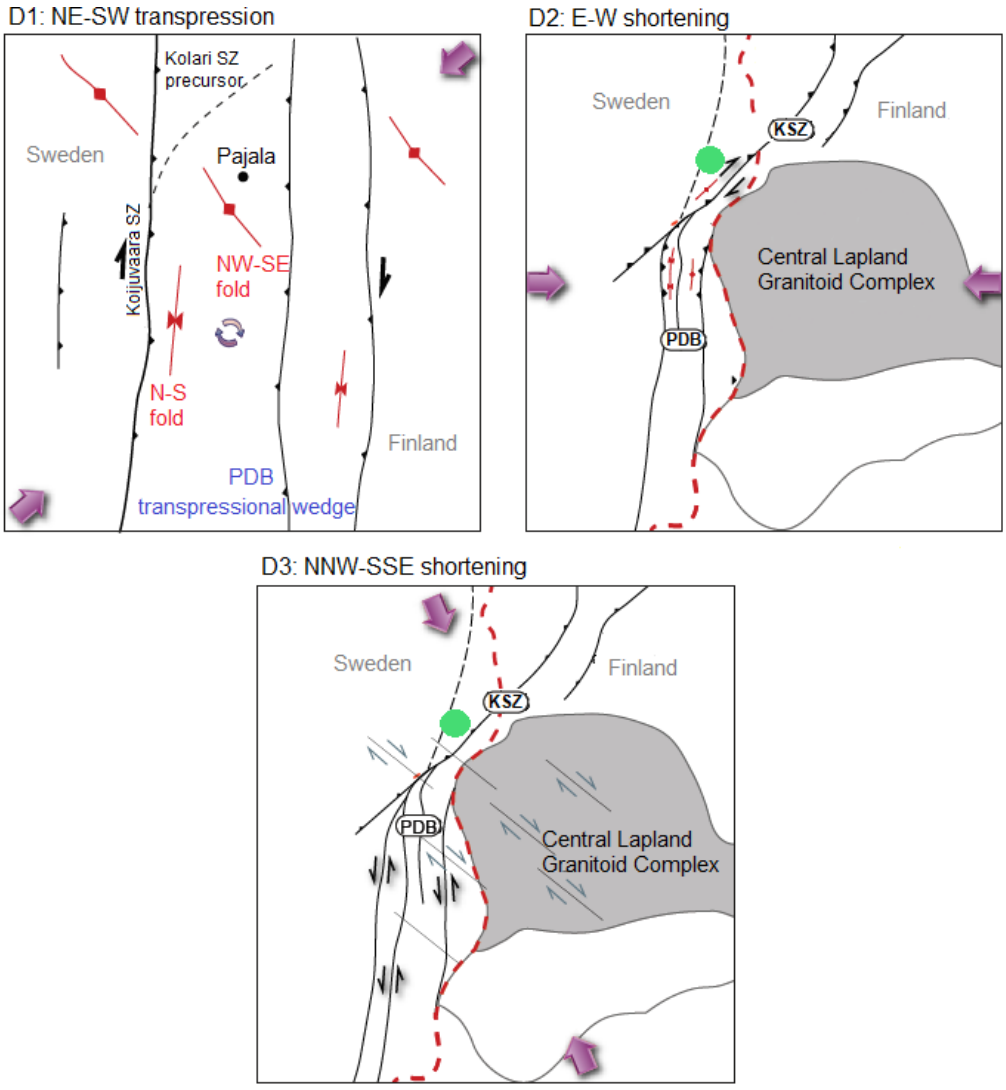

Figure 5. Illustrations of the three main deformation phases affecting the Pajala deformation belt (PDB) and Kolari shear zone (KSZ). Arrows indicate direction of crustal shortening. Red dashed line indicates national border. Green circle shows the location of the Tapuli deposit. Modified from Luth et al. (2018).

3.4 Contiguous deposits

3.4.1 Pajala area

The Sahavaara deposit (Figure 6), historically divided into Stora and Södra Sahavaara, is the second largest iron deposit in the Pajala area after Tapuli. Measured and indicated resources amount to 86.8 Mt with a grade of 39.82% Fe and 1.93% S (Baker et al., 2011). Comparable to Tapuli, the magnetite-skarn mineralisation occurs at the contact between Karelian graphitic schists and carbonate rocks in the footwall, and Svecofennian sedimentary rocks in the hanging wall (Bergman & Hellström, 2020). Although iron grades are considerably higher in the Sahavaara deposit, the elevated concentration of sulphur requires flotation processing for mining to be viable. The current exploitation concession held by KIAB includes the Sahavaara deposit and eventual mining is dependent on the outcome of a pending environmental permit.

The Pellivuoma deposit (Figure 6) is located roughly 15 km west of Sahavaara. The deposit was drilled by SGU during the Iron Ore Inventory Program in the 1960s, and subsequently by Northland in 2008. Based on a 20% iron cut-off grade, the indicated mineral resource totals 33.81 Mt at a grade of 30.15% Fe and 0.56% S, while the inferred resources amount to 50.01 Mt at a grade of 29.75% Fe and 0.99% S (Lindholm, 2009). In accordance with the Tapuli and Sahavaara deposits, mineralisation occurs as a magnetite-rich skarn alteration in the upper portion of Karelian greenstones (Bergman & Hellström, 2020). Other known iron skarn deposits in the Pajala area include Karhujärvi, Ruutijärvi and Suksivuoma (Figure 6), all of which were drilled during the 1960s. Mineral resources have not been fully constrained, but geophysical modelling carried out in 2008, by contract from Northland, suggests over 25 Mt iron resources in the Suksivuoma deposit (Bergman & Hellström, 2020).

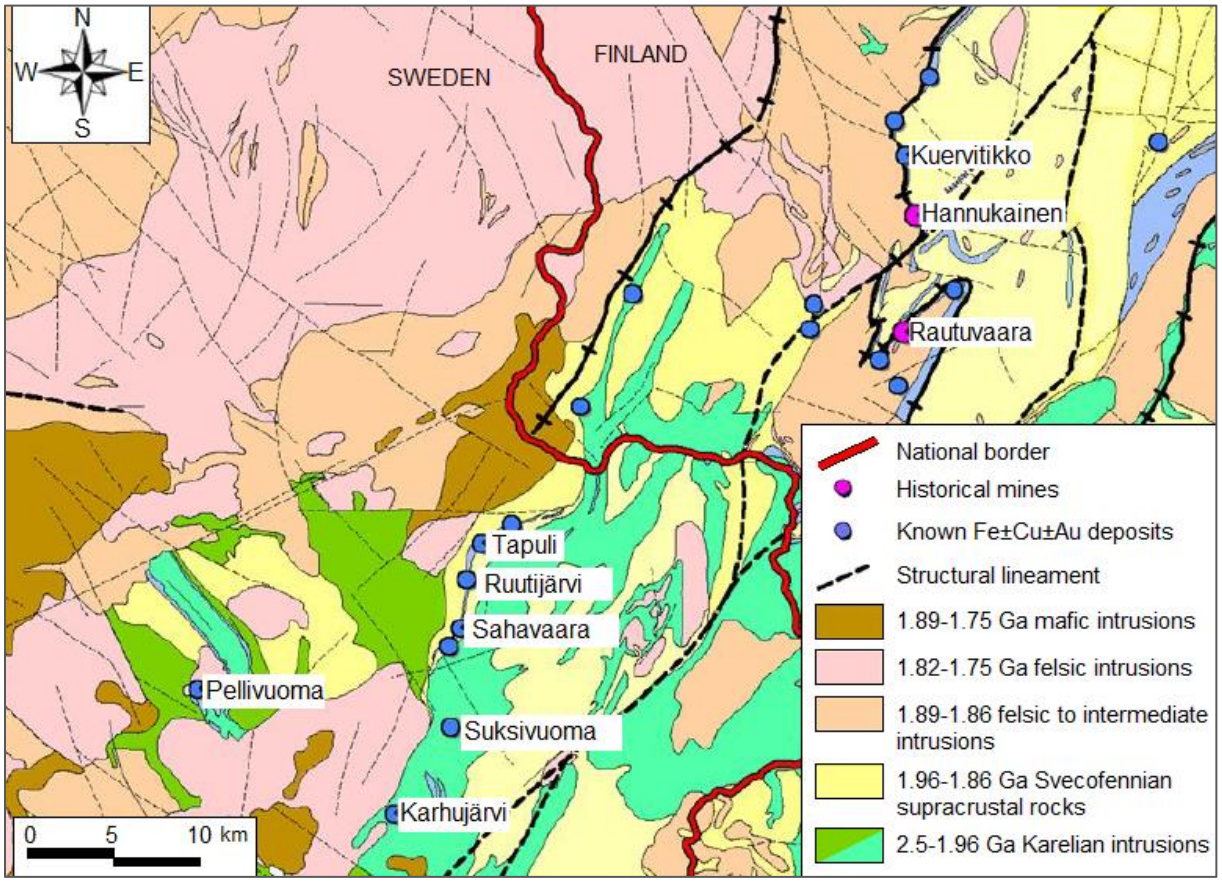

Figure 6. Geological map showing mineral occurrences in the Pajala and Kolari areas. Modified from Northland Resources (2009). Note: ages and allocations of rock units slightly differ from more recent studies.

3.4.2 Kolari area

Several deposits, considered to be of a similar type as the Pajala area counterparts, occur in the Kolari district of Finnish Lapland (e.g., Hannukainen, Rautuvaara and Kuervitikko; Figure 6). These deposits are commonly suggested to belong to a loosely defined but economically important group of iron oxide-copper-gold (IOCG) type deposits (Niiranen, 2005; Moilanen & Peltonen, 2015). The main ore mineral is magnetite and the Hannukainen and Rautuvaara deposits were both mined for iron between the 1970s and 1990s. The Kolari deposits are hosted by clinopyroxene-dominated skarns located within shear and fault zones along the KSZ, although their characteristics are somewhat different from the Kaunisvaara deposits. Contrary to the Pajala area, the Kolari district contain considerably higher concentrations of Cu and Au, which locally grades up to 8.3% and 6.0 ppm, respectively, at the Kuervitikko deposit (Niiranen et al., 2007). These two metals typically occur in sub-economic grades in north-eastern Norrbotten and the IOCG term is only occasionally used in descriptions of the Swedish deposits (Bergman & Hellström, 2020; Moilanen & Peltonen, 2015). Furthermore, the Kolari deposits formed near the contact zone between c. 1.86 Ga Haparanda suite intrusions and >2.05 Ga supracrustal rocks composed of graphite- and sulphide-bearing schists (Niiranen et al., 2007). In the Kaunisvaara area, on the other hand, there is no established correlation between mineralisation and any specific major intrusion. Although not yet identified, such a correlation may still exist.

4 Local geology

4.1 Lithostratigraphy and deformation in the Pajala area

The bedrock in the Pajala area is composed of primarily Paleoproterozoic supracrustal rocks and multiple generations of Svecokarelian intrusive rocks. The bulk of the rocks formed in a volcanic arc environment and were metamorphosed and deformed to variable extent during the Svecokarelian orogeny (Bergman et al., 2001). The supracrustal rocks in the area can be broadly separated between Karelian greenstones and overlying Svecofennian rocks. The Karelian rocks, including similar rocks in the Masugnsbyn area, is referred to as the Veikkavaara greenstone group and occurs at the same stratigraphic level as the Kiruna greenstone group in north-western Norrbotten. The Svecofennian rocks mainly belong to the so-called Sammakkovaara group, which is stratigraphically equivalent to the Porphyrite group to the west (Bergman & Hellström, 2020). The supracrustal rocks are intruded by a series of early to late Svecokarelian intrusions with ages ranging between 1.96 and 1.75 Ga. In a synoptic view, Luth et al. (2018) divided the Pajala area into three distinct geological domains based on lithology, metamorphic grade, and deformation characteristics. These domains are briefly outlined in the following sections.

4.1.1 Suorsa domain

In the Suorsa domain (Figure 7) west of Pajala, the bedrock is composed of variably deformed mafic to intermediate Svecofennian metavolcanic rocks belonging to the Sammakkovaara group. Metamorphic grade is generally lower compared to more central areas within the PDB and ranges from greenschist facies to amphibolite facies (Bergman & Hellström, 2020; Luth et al., 2018). The Suorsa domain borders the western boundary of the PDB, marked by the Koijuvaara shear zone, and is structurally heterogenous with deformation ranging from weakly foliated rocks to extensively sheared mylonites. The supracrustal rocks are intruded by large volumes of intrusive rocks consisting of early Svecokarelian metamorphosed gabbros and diorites (1.96–1.86 Ga) and mid to late Svecokarelian intrusions of granitic composition (1.88–1.75 Ga; Luth et al., 2018).

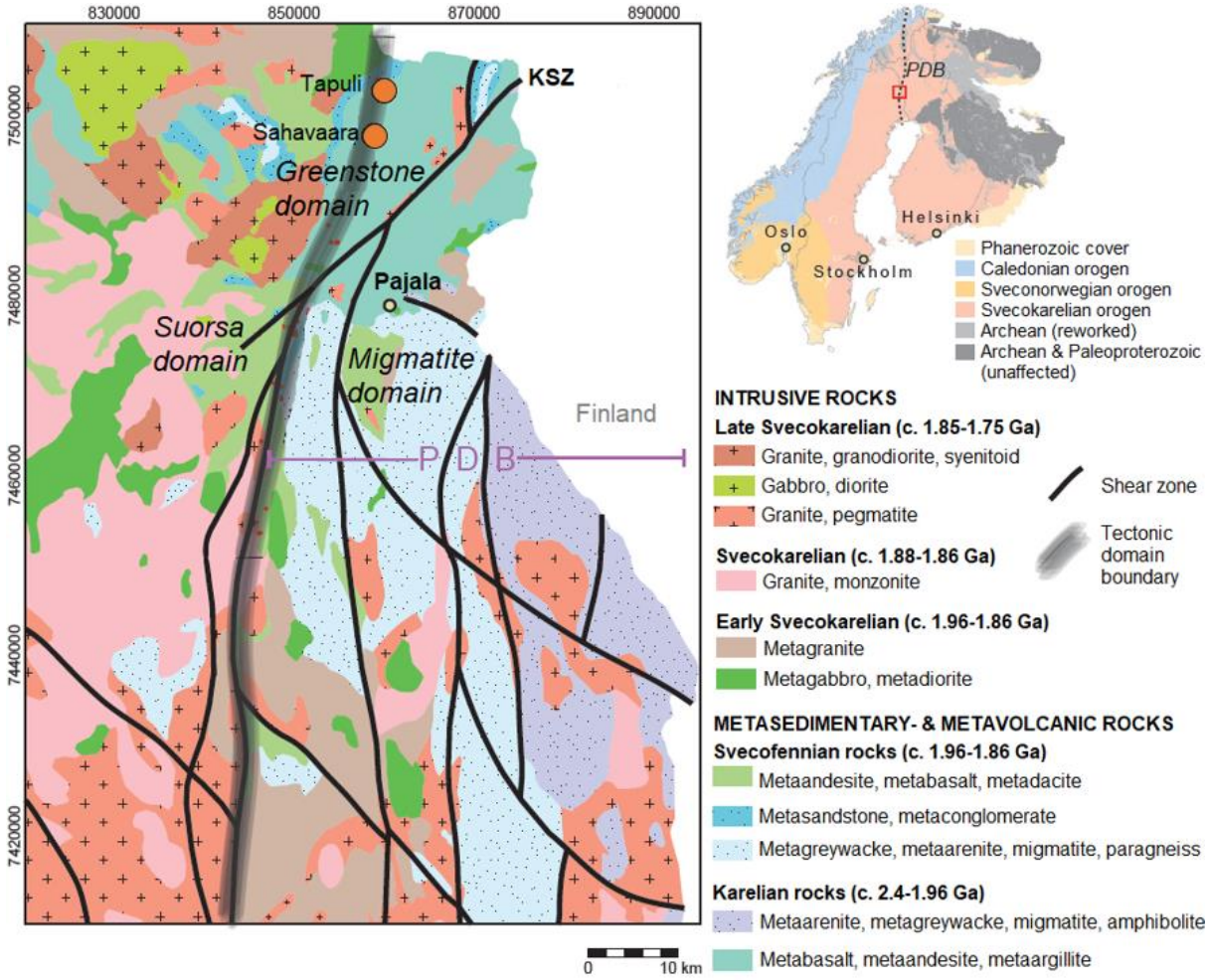

Figure 7. Geological map showing three distinct geological domains in the Pajala area. PDB = Pajala deformation belt. KSZ = Kolari shear zone. Modified from Luth et al. (2018).

4.1.2 Migmatite domain

The Migmatite domain (Figure 7) is located south of Pajala and is characterized by highly deformed Svecofennian metasedimentary rocks. These rocks are primarily composed of migmatitic metasandstone and banded paragneiss formed by high-grade alterations within the PDB (Bergman & Hellström, 2020). The structural pattern is expressed by NNE-SSW to NW-SE trending shear zones and the presence of sillimanite and garnet indicates high-temperature metamorphism reaching amphibolite facies (Luth et al., 2018). Intrusive rocks occur to a limited extent within the domain and are mainly composed of late Svecokarelian granites and pegmatites (1.85 –1.75 Ga).

4.1.3 Greenstone domain

Rocks of the Greenstone domain (Figure 7), north of Pajala, primarily belong to the Veikkavaara greenstone group and are dominated by mafic to ultramafic volcaniclastic rocks overlain by Svecofennian volcanic and sedimentary rocks. The Tapuli and Sahavaara deposits, located within the domain, are associated with graphitic schists and carbonate rocks belonging to the uppermost portion of the Karelian greenstones. The domain overlaps the PDB-KSZ intersection, and the structural trends are dominated by NE-SW oriented folds and shear zones with high-grade metamorphic alterations (Bergman & Hellström, 2020). Based on the occurrence of amphibole, garnet, and diopside, the rocks

have been metamorphosed to amphibolite facies (Luth et al., 2018). Intrusive rocks include early Svecokarelian intrusions of metamorphosed granite and gabbro (1.96–1.86 Ga), as well as a wide range of late Svecokarelian suites, ranging from granite and pegmatite to diorite and gabbro (1.85–1.75 Ga).

4.2 Tapuli deposit lithostratigraphy

A simplified schematic diagram of the deposit-scale stratigraphy of the Tapuli iron skarn, showing the main rock units, is presented in Figure 8. The iron skarn is hosted by Karelian greenstones in the footwall and Svecofennian supracrustal rocks in the hanging wall. Outside the pit area, outcropping rocks occur scarcely as the bedrock is capped by <20 m thick Quaternary deposits consisting mainly of glacial till. The till is typically overlain by a 0.6–5 m thick layer of peat (Palmén et al., 2009).

Different definitions referring to the carbonate rocks in the uppermost portion of the Tapuli footwall occur in the literature. For instance, Luth et al. (2018) used the term *dolomite* to describe the formation, Denisova (2013) referred to it as *dolomitic marble*, whilst Dishaw & Lepley (2021) used both *marble* and *dolomite* in their descriptions. Based on the large variations of Mg grades in carbonate-dominated production drillholes, *dolomitic marble* might be preferable as a broad definition. However, for the sake of simplicity, the term *dolomite* is applied in this thesis.

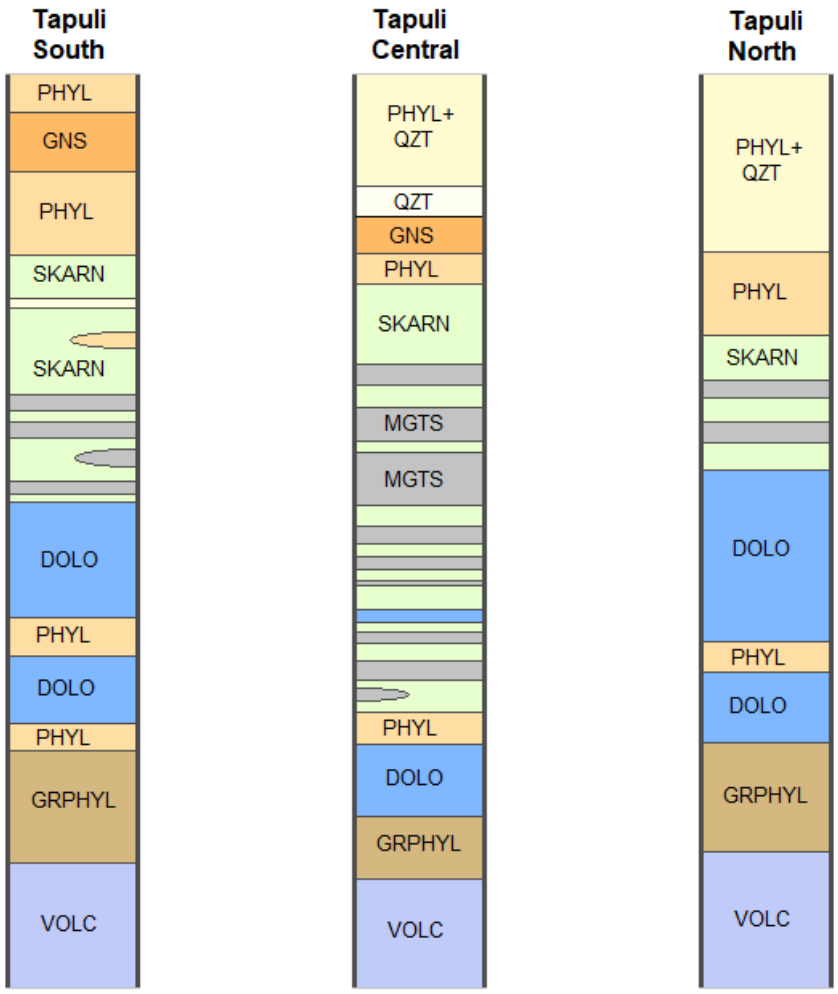

Figure 8. Simplified stratigraphic diagram of the Tapuli deposit based on drill core logs. PHYL = phyllite, GNS = paragneiss, QZT = quartzite, SKARN = magnetite-deficient skarn, MGTS = magnetite-rich skarn, DOLO = dolomite, GRPHYL = graphitic phyllite, VOLC = volcanic basement rocks.

4.2.1 Footwall

The lowermost portion of the Tapuli stratigraphy belongs to the Veikkavaara greenstone group and is composed of thinly bedded phyllite overlain by a unit of foliated dolomite (Baker & Bonson, 2013; Bergman & Hellström, 2020). Locally, the phyllite grades into graphitic phyllite at stratigraphically higher levels, where disseminated graphite typically occurs together with plagioclase, amphibole and minor titanite (Lindroos et al., 1972; Denisova, 2013). Sulphides, mainly pyrite and pyrrhotite, are abundant, particularly in the graphitic zones and appear as fine-grained disseminations or coarse-grained inclusions associated with calcite veins (Denisova, 2013). Small intercalations of dolomite occur in the upper parts of the phyllite and the contact between the two units is transitional and characterized by interbedding.

The dolomite forms the footwall to the skarn mineralisation and can be followed throughout the extent of the deposit with a fluctuating thickness of 20–150 m (Baker & Bonson, 2013). The contact between the mineralisation and footwall is gradual and carbonates and skarn are frequently mixed within a transition zone spanning over a few meters (Figure 9). Layers of dolomite, up to several meters in thickness, can be found locally within the skarn. Pyrite, pyrrhotite, and minor chalcopyrite occur as unevenly distributed veinlets and disseminations throughout the dolomite (Denisova, 2013).

Figure 9. Transitional contact between the foot wall dolomite (left) and skarn alteration (right), Tapuli Central pit.

4.2.2 Mineralisation

The mineralisation is comprised of a highly variable magnetite-rich skarn alteration which largely overprints the footwall dolomite (Baker et al., 2011). Mineralised zones appear as NE striking lenses and bands, dipping concordantly with the local stratigraphy 45–60° to the NW. The mineralisation continues from the central portion of the deposit, forming elongated extensions to the NE and SW with a total length of roughly 2 km (Figure 10). The thickness of the skarn alteration ranges between

20 and 250 m and correlates with the thickness of the dolomite. Generally, where the skarn alteration is thick the dolomite is thin and vice versa. Still, the combined thickness of the two units is consistently around 250 m throughout the deposit (Baker & Bonson, 2013). The extent of the mineralisation has been outlined by exploration drilling to a maximum of 300 m below the surface, so the vertical reach of the deposit is not fully constrained (Baker et al., 2011).

Three major types of skarn assemblages have been distinguished in the deposit: clinopyroxene-tremolite alteration, magnetite-actinolite alteration, and serpentine alteration (Figure 11; Bergman & Hellström, 2020; Baker & Bonson, 2013). Dishaw & Lepley (2021) suggested that the clinopyroxene-tremolite alteration predates the magnetite-actinolite counterpart, while the serpentinization represents the final alteration stage. The latter, thus, postdating the main mineralisation event. Nevertheless, magnetite-rich zones occur in all three major skarn assemblages and in the highest-grade portions of the deposit, serpentine is the dominant gangue mineral (Dishaw & Lepley, 2021). The protolith for the mineralisation has not been conclusively determined, but local zones of biotite- and albite-rich alteration in the skarn indicates that the protolith may have been an aluminium-rich silicate rock rather than dolomite (Dishaw & Lepley, 2021).

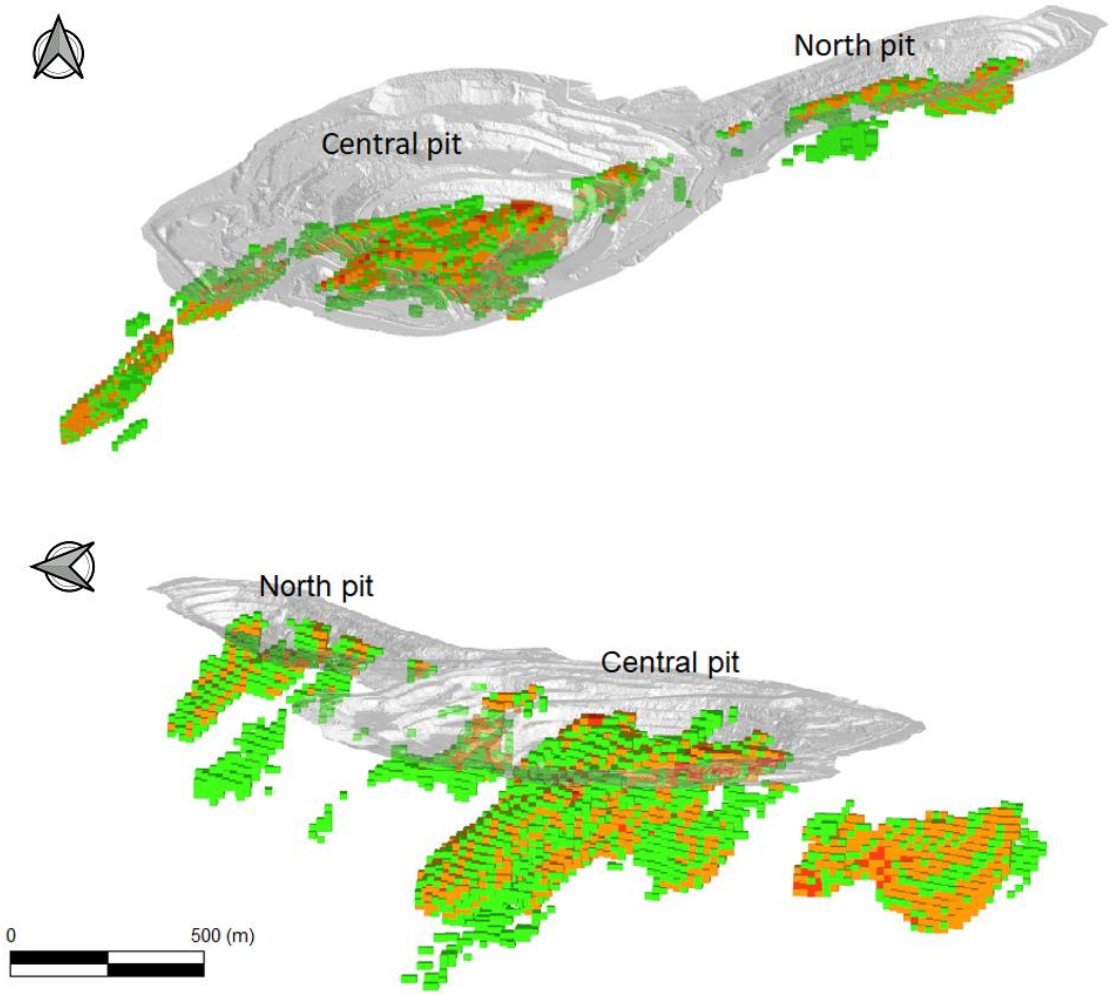

Figure 10. Current pit design superimposed on the resource block model. Blocks are coloured by iron grade (green: 20-25% Fe, orange: 25-35% Fe, and red: >35% Fe). The south-western mineralised lens is not included in the present exploitation concession. Upper: inclined view from the south. Lower: inclined view from the west.

According to Dishaw & Lepley (2021), the average sulphur grade of the mineral resources amounts to 0.4% S. However, sulphides are unevenly distributed throughout the mineralisation and individual bench-scale samples from production drill holes in the mineralised zones occasionally contain up to 10% S. Pyrite and pyrrhotite (Figure 12) are the main sulphide minerals along with minor chalcopyrite. Cu concentrations are generally low in the sulphide bearing zones but still contain a few hundreds of ppm (Dishaw & Lepley, 2021). Sulphur grades typically increase with depth and the highest concentrations are found within the lowermost layers near the footwall contact (Figure 13). Similarly, the pyrrhotite-pyrite ratio increases with proximity to the footwall and, particularly, close to the graphitic phyllite (Denisova, 2013). Closer to the hanging wall, pyrite appears to be the dominating sulphide, with pyrrhotite occurring only sporadically.

Figure 11. The three major types of skarn alterations in the Tapuli deposit: Clinopyroxene-tremolite skarn (A), magnetite-actinolite skarn (B outside red markers) and serpentinite skarn (B inside red markers).

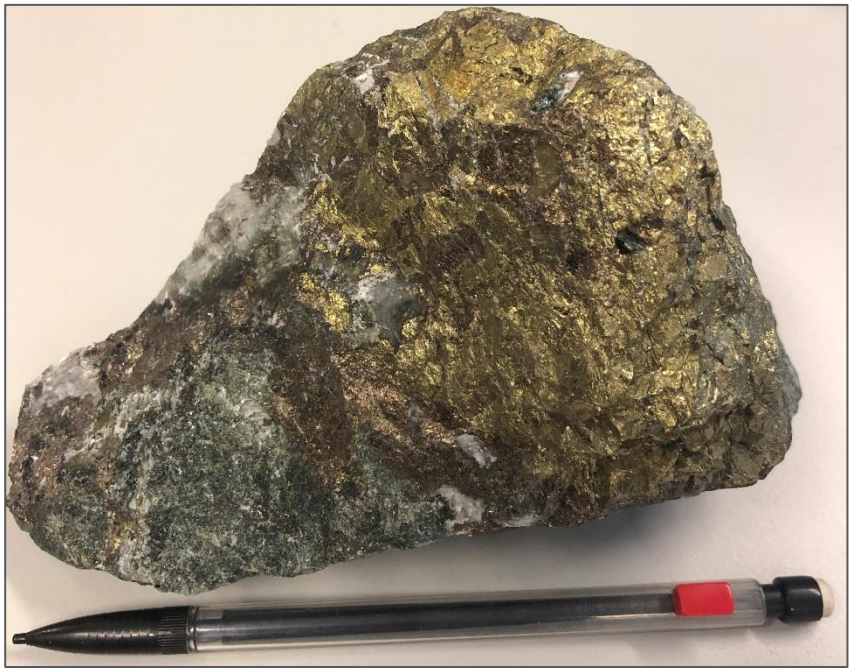

Figure 12. Pyrite (yellow) and pyrrhotite (bronze coloured) in rock sample collected from the skarn-dolomite contact, Central pit.

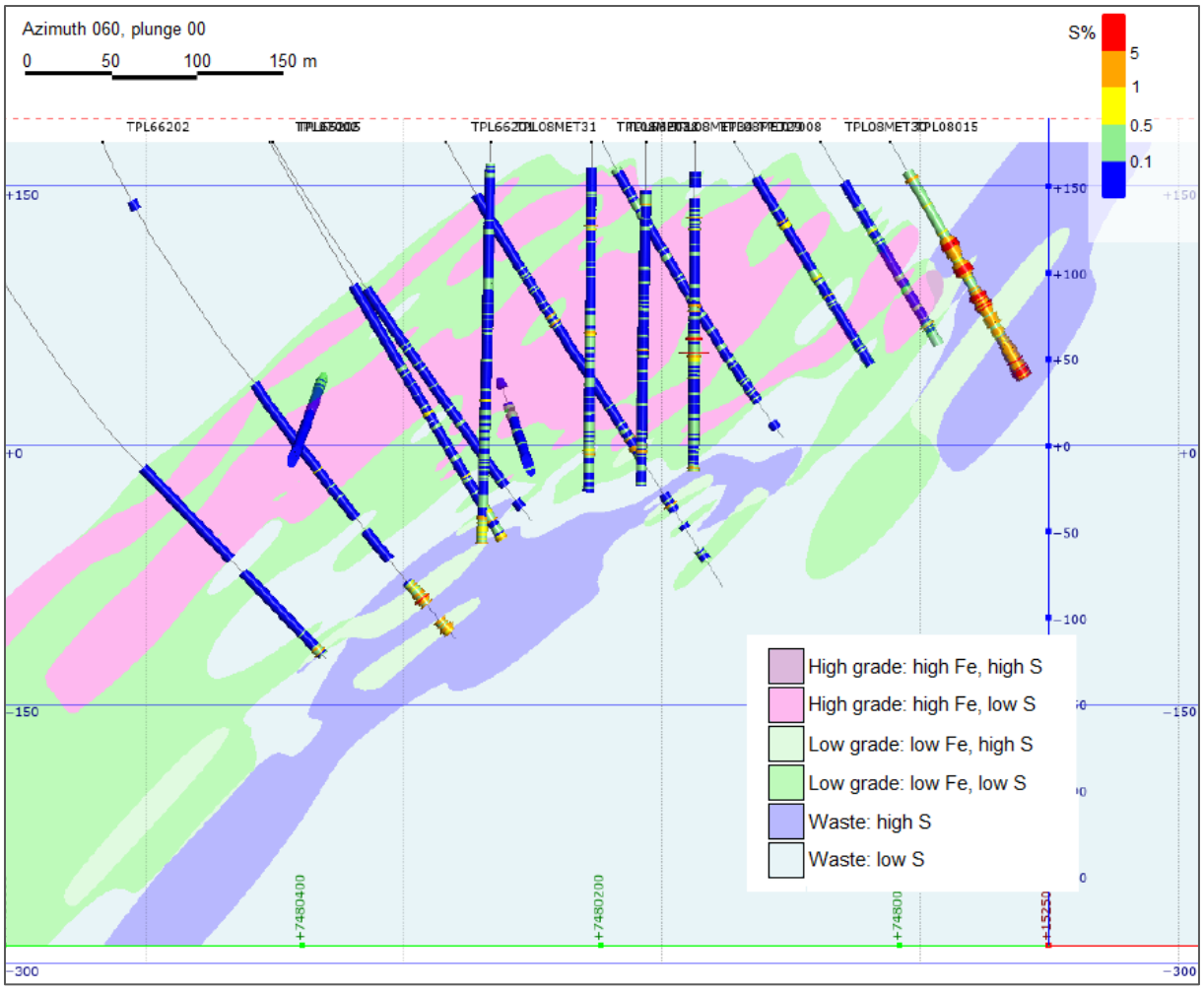

Figure 13. Cross-section through the central portion of Tapuli showing meshes of different grade domains. Cut-off grades are 10% and 25% Fe, and 0.5% S. Drillholes are coloured by S%. Modified from Dishaw & Lepley (2021).

4.2.3 Hanging wall

A Svecofennian metasedimentary sequence, belonging to the Sammakkovaara group, forms the hanging wall to the mineralisation. The sequence consists of layered quartzite, phyllite and quartzitic phyllite, or higher-grade equivalents such as mica schist and biotite gneiss (Bergman & Hellström, 2020). Sedimentary structures are well preserved with distinct bedding being observable in many of the rocks. The contact between the skarn and the metasedimentary rocks is transitional and typically spans over a few meters. With exception to the transition zone, no sulphides have been observed in the hanging wall sequence. This observation is accordant with previous mineralogical studies of the deposit (e.g., Lindroos et al., 1972 and Denisova, 2013) and is further supported by the low sulphur grades seen in bench-scale samples from production drill holes.

4.2.4 Intrusions

Several mafic dikes, with a typical thickness of <5 m, crosscut the stratigraphy at high to intermediate angles in both pits (Figure 14). Microscopic studies by Denisova (2013) indicate that the mineralogy mainly consists of actinolite, biotite and plagioclase, with minor titanite and magnetite. The dikes are pervasively altered, and the main alteration minerals have been identified as chlorite, phlogopite and scapolite, occasionally with sulphide overprinting (Denisova, 2013).

Figure 14. Mafic dikes in the footwall dolomite, Central pit. The lower dike is offset by a steeply dipping fault.

4.3 Tapuli deposit deformation

4.3.1 Ductile deformation

The Tapuli deposit is located within the limb of an inclined isoclinal anticline on the westernmost margin of the Koijuvaara shear zone, where the PDB is intersected by the KSZ (Baker & Bonson, 2013; Luth et al., 2018; Figure 7). The central and most massive part of the deposit is situated along the major fold axis, distinguished by Baker & Bonson (2013) through 3D modelling of the mineralisation-footwall contact (Figure 15). The axial plane of the Tapuli anticline plunges towards the NW with an approximate orientation of 60/305 (dip/dip direction). The NE-SW strike of the fold axis is consistent with the structural trends within the PDB-KSZ intersection, as described in section 3.3. Baker & Bonson (2013) considered the deformation to be in accordance with semi-regional shearing and dextral transpressional deformation accommodated by the PDB. The same authors also suggested that the mineralisation formed after the main deformation event, based on the observation that the skarn geometry is controlled by pre-existing deformation fabrics in the host rocks. The presence of relatively undeformed porphyroblasts, overgrowing mylonitic rocks in the hanging wall, implies that ductile deformation of the hanging wall predates the skarnification (Baker & Bonson, 2013).

Generally, ductile deformation appears to be more pronounced in the hanging wall compared to the skarn and footwall dolomite. This may, at least partially, be related to the fact that significantly more of the hanging wall is exposed in the pits. Many rocks show signs of extensive ductile strain and several fold structures, typically with an amplitude of a few meters, can be observed in the hanging wall in both Central and North pit (Figure 16). Baker & Bonson (2013) reported moderately developed stretching

lineation, aligned sub-parallel to the dip, as well as signs of boudinage in the hanging wall sequence. Although these fabrics could not be observed in field, well-developed foliation is apparent in many of the hanging wall rocks. Regarding deformation of the skarn, Baker & Bonson (2013) identified small isoclinal folds in the compositional banding consisting of magnetite-rich and magnetite-poor layers. Yet, the same authors determined the overall skarn assemblages to be neither strongly foliated nor folded in nature. Large portions of the skarn remain devoid from deformation fabrics, which indicates that the skarnification largely post-dated and, therefore, likely overprinted any pre-existing ductile deformation in the host rocks. Furthermore, the footwall dolomite, which is broadly exposed along the south-eastern wall in the Central pit, is typically deficient of distinct folding. Still, a strong planar foliation, oriented similarly as the hanging wall foliation, can be observed.

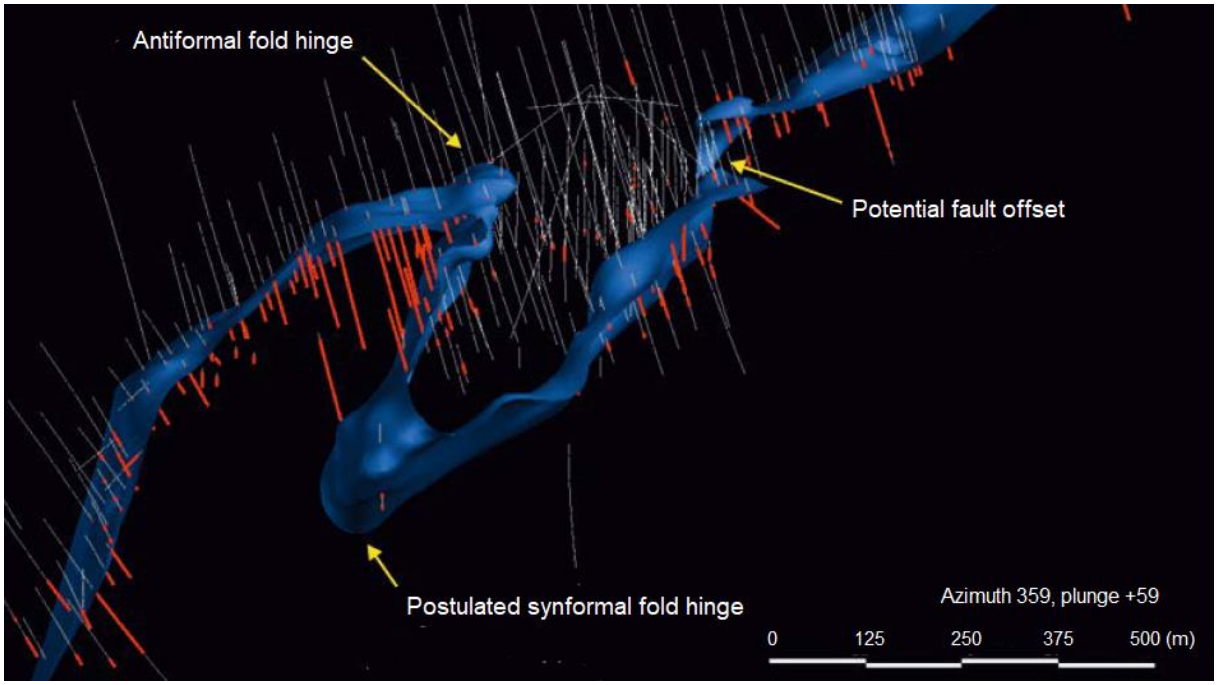

Figure 15. Modelled surface of the skarn-dolomite contact (blue), interpreted as a north-plunging fold hinge. Intersections of dolomite, obtained from core logging, are displayed in red. Modified from Baker & Bonson (2013).

Figure 16. Fold structures with an amplitude of roughly 1 m in the hanging wall sequence, North pit.

4.3.2 Brittle deformation

Several portions of the pit walls are intensely fractured, particularly in the uppermost benches, and large faults with steep to gentle dips crosscuts the stratigraphy at numerous locations. A general sense of displacement is difficult to determine due to brittle conditions and a scarce occurrence of reliable indicators. Nevertheless, Baker & Bonson (2013) reported reverse displacement of a mafic dike along the northern wall in the Central pit of roughly 8 m. This is consistent with the displacement of moderately dipping reverse faults observed in both Central and North pit (Figure 17). In addition, Baker & Bonson (2013) were able to correlate distinct breaks, perceived in aerial and ground-based magnetic data, with offsets in the skarn-dolomite contact observed in drill cores. The authors interpreted these breaks to be the result of steep reverse or strike-slip faulting.

Fault zone intervals attained from core logging by SRK Consulting and Northland, respectively, are shown in Figure 18. The fault zones typically range in width between 0.5 and 5 m, are often brecciated and contain abundant chlorite, actinolite, and clay mineral alterations (Baker et al., 2011). No oriented core data is included in these logs but during the 2009 hydrological study (see section 2), acoustic televiewer and video logging of 27 drillholes were conducted by Pöyry. In total, 1,720 m of oriented fracture log was produced, including orientations of 12,768 fractures (Vaittinen et al., 2009). Four main orientational trends were distinguished, of which SW striking fractures with steep dips to the NW were dominant. A conjugate orientation, with strikes to NE and gentle to moderate dips to the SE, were also observed. Additionally, intersecting orientations dipping towards the SW or NE were found with SE and NW trending strikes respectively. All four orientations were encountered throughout the extent of the studied rock mass, including mineralisation, hanging wall, and footwall. Rock Quality Designation (RQD), which is a rough measure of fracture frequency and core recovery, was performed and evaluated by Palmén et al, (2009) on the same 27 drillholes (Figure 19). The results showed a significant decrease in RQD value in the uppermost 50 m of the cores, indicating increasingly fractured rocks near the surface. A similar trend can also be distinguished in the Northland core logs (Figure 18).

Groundwater discharge in the mining pits is a recurring issue which causes occasional delays in drilling and loading, particularly during springtime. Since mining commenced at Tapuli in 2012, no detailed investigations on the synergy between local groundwater flows and bedrock fractures have been made.

Figure 17. Moderately dipping reverse fault with a displacement of approximately 5 m in the North pit hanging wall.

The 2009 Pöyry study showed, however, that flow rates were greater in the uppermost part of the hydrological drillholes (Perman et al., 2009). This implies a more hydraulically conductive rock near the surface, which is consistent with available core logs and RQD data (Figure 18 & 19). Still, groundwater seepage from pit-wall fractures can be observed on practically all bench levels (amounting to roughly 160 m of vertical extent).

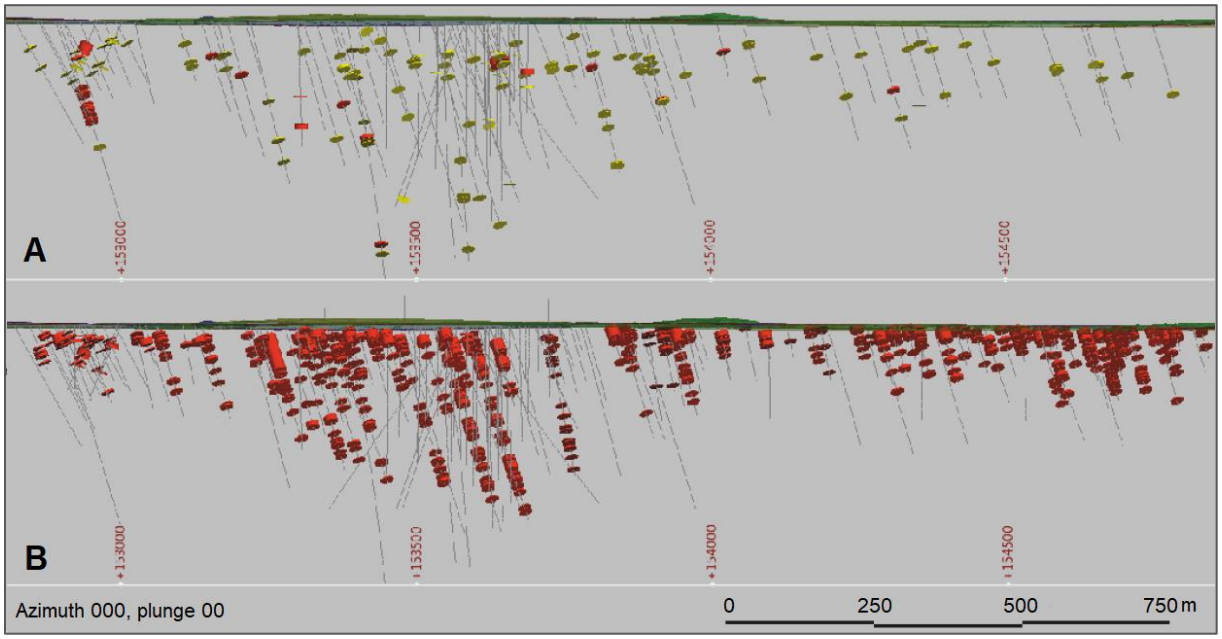

Figure 18. North-facing view of Tapuli drillholes showing fault zone intervals logged by SRK Consulting (A) and Northland (B). Fault zones logged by SRK Consulting have been subdivided into minor (yellow) and major (red) fault zones. Modified from Baker & Bonson (2013).

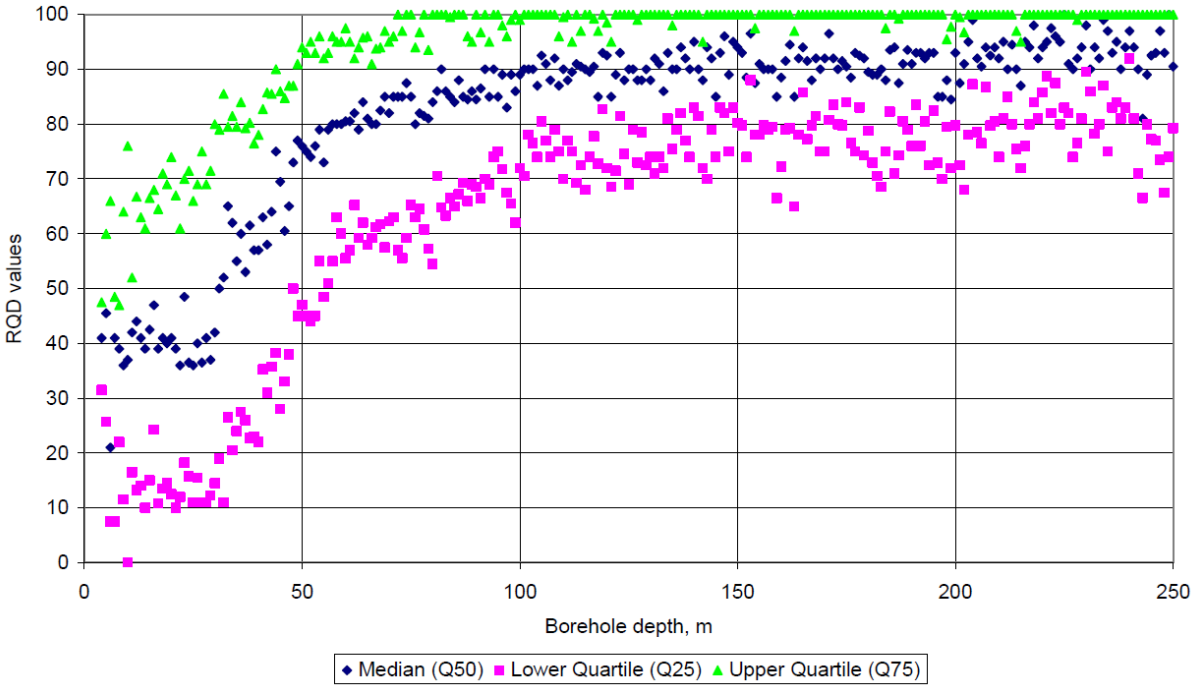

Figure 19. RQD median, upper, and lower quartiles for 1 m depth intervals plotted against drillhole depth. RQD-values are significantly lower closer to the surface but stabilize around 100 m depth. From Palmén et al. (2009).

5 Method

In this project, brittle deformation within the study area was mapped and characterized by analysing geophysical and structural geological information. The main work was divided into two stages. The first stage included interpretation of pre-existing geophysical data, aimed to outline the structural framework in a semi-regional perspective. During the second stage, detailed structural measurements of the pit walls were collected and evaluated in correlation with the geophysical interpretations.

5.1 Interpretation of geophysical data

5.1.1 Principles of lineament analysis

Lineament analysis is a technique commonly applied for mapping and characterizing possible deformation zones in the bedrock. A lineament is an expression of an underlying geological structure such as a fault, shear zone or dike, manifested as a linear feature at the surface. Moreover, a lineament can refer to an interpreted one-dimensional line, which is drawn in relation to linear or semi-linear features observed in a map or data set. The term was more precisely defined by O´Leary & Friedman (1978) as:

"A map able (at 1:25,000 and smaller scale), simple or composite linear feature of a surface, the parts of which are aligned in a rectilinear or slightly curvilinear relationship, and which differs from the pattern of adjacent features and presumably reflects a subsurface phenomenon".

Historically, lineament analyses were based solely on topographic information, but lineaments are often also perceivable in geophysical data such as magnetic or electromagnetic maps, as well as aerial and satellite imagery. By using geophysical techniques applied for structural analysis of the ground surface, it is possible to map features which are not outcropping but occurring at depth. Typically, geophysical measurements are used to support the correlation between features in the terrain, observed in topographic data, and characteristics of the underlying bedrock. In cases where the bedrock surface is obscured by overburden, geophysical data can be used as an analogue to topographic data in structural analyses. Interpretations based on both topographic and geophysical information are desirable in the characterization of a feature as the two data types complement each other.

Brittle deformation (e.g., faults and fault zones) is commonly manifested in topographic and geophysical maps as linear features of topographic lows, magnetic lows, and electrical conductivity highs. This is a result of changes to the physical, chemical, and mechanical properties of the rocks introduced by the deformation. For instance, the magnetic susceptibility of the bedrock is governed by the content of magnetic minerals such as pyrrhotite and, most importantly, magnetite. Magnetite is a strongly magnetic iron-oxide mineral which occurs to varying extent in a broad range of crystalline rocks. Faulting of the bedrock may expose rock material along the fault planes to weathering agents such as air and water. Under such conditions, magnetite (Fe_3O_4) will typically oxidize into the significantly less magnetic mineral hematite (Fe_2O_3) (Henkel & Guzman, 1977). Consequently, faults and fault zones are often embodied in magnetic maps as linear elements with a lower magnetic susceptibility compared to the surrounding bedrock.

Since most silicate minerals are poor conductors (Karato & Wang, 2013), faults that function as groundwater conduits will generally exhibit an increase in electrical conductivity compared to the host rocks. This distinction is caused by the relatively higher conductive properties of the groundwater in relation to most rocks and minerals. Graphite (C), however, is a strongly conductive native mineral with a conductivity value reaching several magnitudes higher than water (Helmenstine, 2020). Therefore, the electromagnetic anomalies produced by water-bearing fractures in geophysical data sets can effectively be indiscernible in the presence of graphite-rich rocks. Moreover, thick layers of overburden not only masks geological information in the bedrock topography but can also influence the electromagnetic

signature, particularly if conductive sediments, such as soil or clay, contain considerable volumes of pore fluids. Conductivity highs are therefore often related to a thickening of the overburden and may, when appearing in a linear or sub-linear form, indicate sediment-filled depressions in the bedrock generated by faulting (Degnan et al., 2001).

It is important to note that lineaments interpreted from topographic or geophysical data only constitutes an indication of a possible deformation zone. To establish the actual existence of such, geological evidence from mapping of outcropping rocks and/or cores from drillholes are required.

5.1.2 Input data and workflow

Topographic and geophysical data sets were combined in the geographic information system (GIS) software QGIS (3.10.7). A digital elevation model (DEM), with a 50x50 m resolution obtained from Lantmäteriet, was superimposed onto magnetic and electromagnetic maps collected by GTK during the 2006 Pajala airborne geophysical survey (see section 2). The survey, which defines the extent of the study area, was conducted with a 100 m line spacing and an approximate survey direction of WNW-ESE. The acquired measurements include several filtrations of total magnetic field intensity, as well as 0.9 kHz and 25 kHz electromagnetic data from slingram separated into real and imaginary components. Additional information applied included satellite imagery and a map of local powerlines.

The data sets were first examined individually where anomalies specific for each measuring technique were identified. To allow correlation between different measuring techniques, the results were then reviewed and interpreted jointly. By doing so, interpretations were made with consideration to all the available data. Emphasis was placed on the topographic and magnetic maps (Figure 20), with a complementary implementation of the electromagnetic data. Based on the certainty of the interpretation, lineaments were sorted into a simple binary hierarchy: confident and less confident. The former category applying to lineaments which could be observed in at least two different data types, as well as lineaments perceivably cross-cutting or displacing geological units. Inferred lineaments and lineaments observed in only one data type were allocated to the latter category.

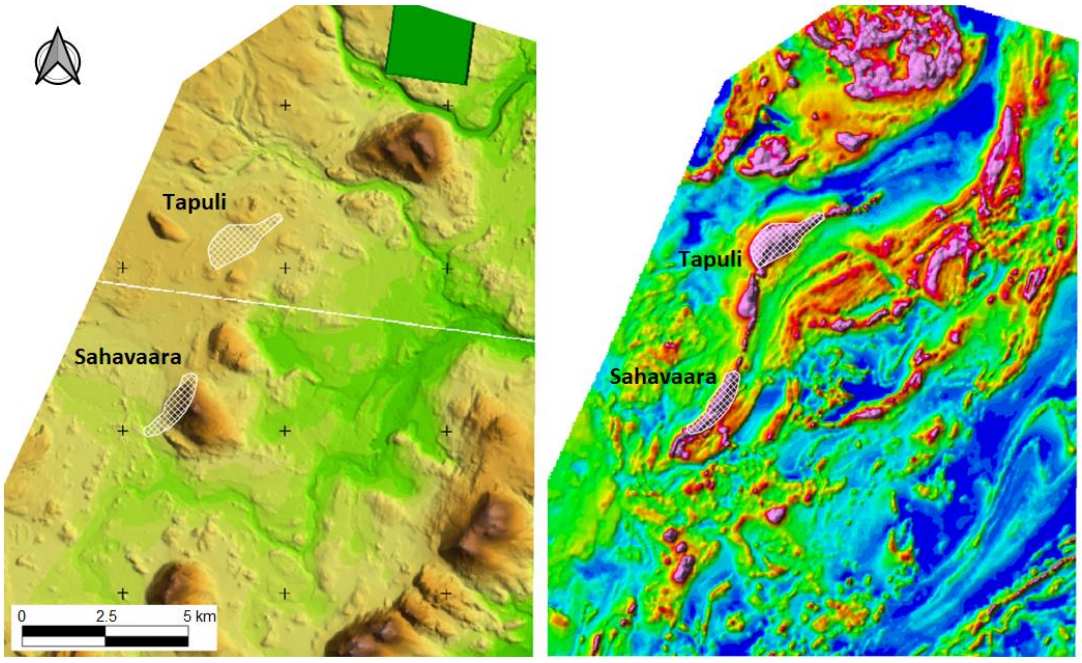

Figure 20. Digital elevation model (© Lantmäteriet [I2014/00579]) and linear magnetic map of the study area.

5.2 Detailed structural analysis

Because of the magnetic field generated by the Tapuli iron-mineralisation, the strike of geological structures within the pit area could not be measured conventionally with a compass. Instead, strike and dip measurements were obtained through software-based operations applied to a point cloud-generated 3D model. A point cloud is a number of data points in space, typically produced by 3D scanning or photogrammetry, where each data point is tied to a set of cartesian coordinates (x, y, z). Although a point cloud can be viewed directly, it is often converted into a 3D model through a process referred to as surface reconstruction (Guo et al., 2020).

Accordingly, georeferenced photography of the pit area was collected using a drone (Figure 21) and imported into the photogrammetry software Pix4Dmapper (4.6.4) from which a point cloud was generated. Using the surface reconstruction method, a 3D model of Central pit (Figure 22) was produced from the point cloud and imported into the software package PointStudio (9.1.0.15742). The model was then used to locate and visualize fault zones by analysing the pit walls in 3D. In cases where distinct fault planes could be observed, a polygon (representing a theoretical plane) was fitted to the fault planes using the fit-plane algorithm in PointStudio (Figure 23). Resultantly, strike and dip measurements could be obtained from the orientations of the fitted polygons using the computer-aided design (CAD) software Deswik.CAD (2020.2).

Although this measuring technique is unaffected by the magnetic properties of the mineralisation, there are instead restraints related to the nature of the 3D model. The relatively limited resolution restricted measurements exclusively to fault planes large enough to not only be distinguishable, but to also express an apparent orientation. Fault planes with sides smaller than roughly 1 m were reproduced in the model by very few, and occasionally outlying, datapoints. Consequently, reliable measurements could not be attained for such planes using the fit-plane algorithm. This drastically decreased the number of available measurements in comparison to using conventional measuring techniques. Moreover, to accurately reproduce an irregular surface using the surface reconstruction method, the input photography should preferably be taken orthogonally to the surface (i.e., the pit walls). Since the model was based on drone

Figure 21. Drone used to collect input photography for the 3D model.

photography taken at an overhead angle to the pit walls, downward facing fault planes were not reproduced and therefore not included in the measurements. The overhead position of the drone also influenced the vertical resolution of the model since the angle between the drone and pit walls decrease with a reduction in pit elevation (approaching a parallel state). Lower pit benches were thus reproduced with a reduced level of detail which largely restricted measurements to the uppermost benches.

Brittle deformation which fails to exhibit distinct planar structures, such as brecciated or crushed zones, are likely to be overlooked by this approach. It should therefore be noted that the results of the structural analysis are derived exclusively from *planar* structures (i.e., faults and fault zones), and do not necessarily include other expressions of brittle deformation that can influence the mechanical strength and hydraulic conductivity of the rock mass.

Figure 22. 3D model of Tapuli Central pit generated from drone photography and surface reconstruction. The diameter of the pit is roughly 500 m.

Figure 23. Schematic illustration showing a polygon fitted to the orientation of an exposed fault plane. The method allowed for strike and dip data to be acquired without interference from the magnetic properties of the mineralisation.

6 Results

6.1 Lineament analysis

A total of 217 lineaments were interpreted and digitized using the available data, of which 69 were considered confident and 148 as less confident interpretations (Figure 24). Individual lineaments were not sorted according to data type, resulting in all 217 lineaments representing interpretations that integrate information from the available datasets (referred to as combined lineaments). Lineament geometries were digitized with the ambition to only reflect features observed directly in the data. No extrapolation or linking of neighbouring lineaments were therefore performed.

Overall, the lineaments are evenly distributed across the study area, with a minor decrease in density in the south-eastern part. Lineament lengths range from 380 to 8,390 m but are typically in the order of 1,000 to 2,000 m, with four examples extending more than 5,000 m. An orientation analysis of all lineaments indicates at least two dominant orientations: NW-SE to NNW-SSE, and NE-SW to NNE-SSW. Approximately 54% of all lineaments are found in the NE-SW to NNE-SSW oriented group, and roughly 44% in the group oriented NW-SE to NNW-SSE. Lineaments oriented either N-S or E-W constitute the remaining ~2%. A summary of the orientation analysis is presented in Table 2.

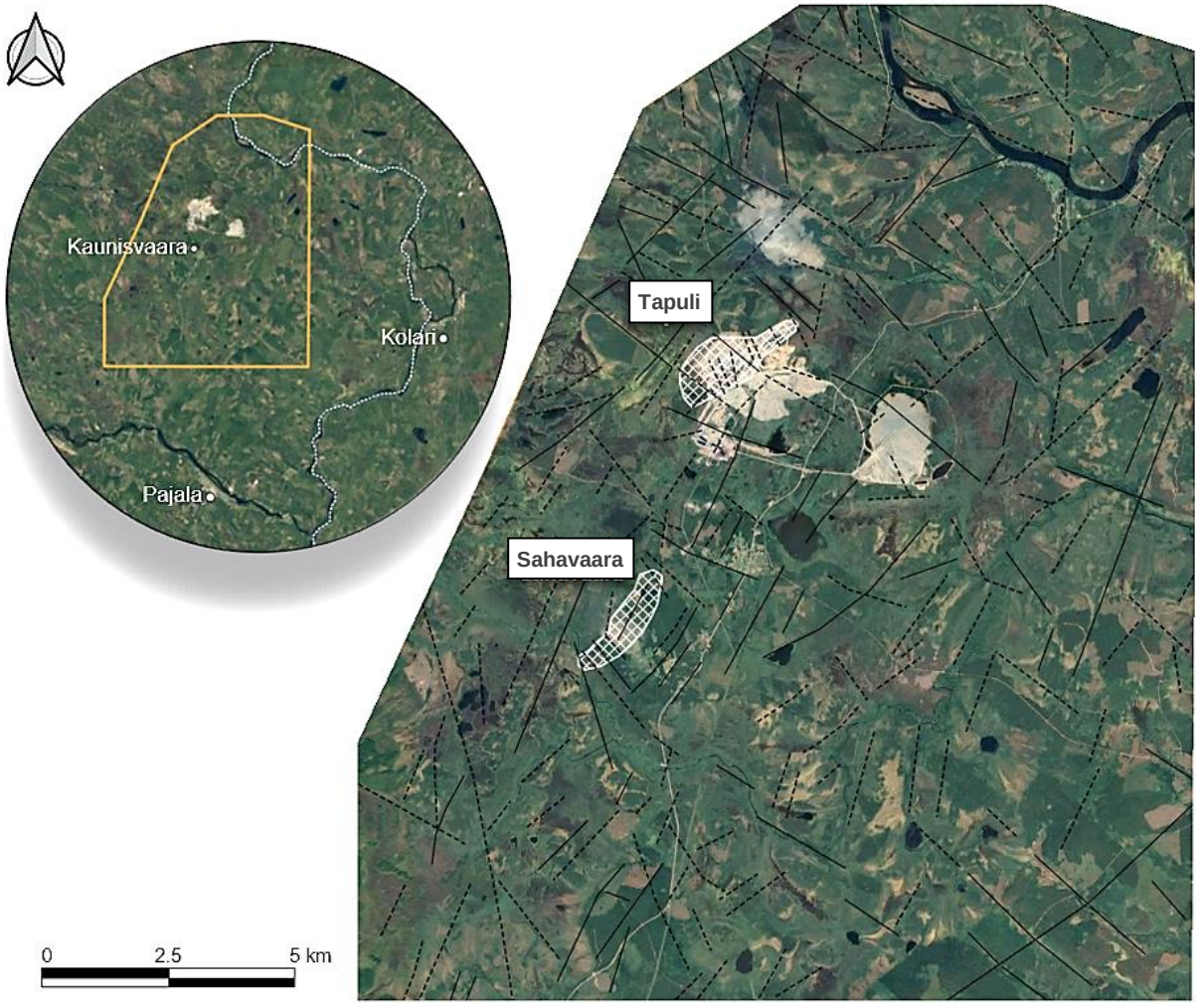

Figure 24. Satellite image of the study area showing a total of 217 interpreted lineaments. Confident interpretations are shown in solid black lines and less confident interpretations are shown in dotted black lines.

Table 2. Summarized results of the lineament orientation analysis.

Orientation	Confident	Less confident	Total
NW-SE to NNW-SSE	33	62	95
NE-SW to NNE-SSW	36	82	118
Other	0	4	4

The two dominant groups are proportionately distributed between confident and less confident interpretations. For the NW-SE to NNW-SSE oriented group, confident interpretations constitute 35%, and less confident interpretations 65% of the total lineaments in that group. The same distribution for the group oriented NE-SW to NNE-SSW are 31% and 69%, respectively. Generally, confident interpretations occur more frequently in the northern half of the study area, with exception to the north-eastern part. Less confident interpretations are more uniformly dispersed but with a minor decrease in frequency in the central and south-eastern parts.

In the following sections, the findings are reviewed individually for each data type. A general discussion on the approach and outcome is provided, accompanied by a brief description of selected lineaments or noteworthy features deemed to hold additional significance.

6.1.1 Topographic data

The two topographic maps used for the analysis included artificial hill shading from the northwest (enhancing NE-SW oriented structures) and from the northeast (enhancing NW-SE oriented structures), both of which were used in parallel. The interpretations were based on the conception that deformation zones have eroded more extensively than the surrounding bedrock, and therefore manifest themselves as valleys or depressions in the topography. In addition, linear contrasts in elevation may in many cases be caused by vertical displacement along a fault plane and can therefore indicate the presence of brittle deformation. Accordingly, lineaments interpreted from the topographic data were identified as either linear topographic lows or sudden and extensive discrepancies in elevation.

The most distinguishing features in the topographic data are NW-SE oriented structures (Figure 25), some of which can be observed cross-cutting areas of topographic highs, such as hills or ridges. In the south-eastern map area, three NW-SE oriented lineaments with an average length of roughly 3,000 m were interpreted exclusively from the topographic data based on such observations. Similarly oriented lineaments transect a topographic bulge in the northern map area but were considered less confident interpretations given the absence of both an apparent displacement and a correlation with the other data types. Several lineaments were also co-interpreted from smaller (<1,000 m) topographic structures, oriented mainly NNE-SSW, observed at various locations.

The central and northwestern parts of the map area, including the Tapuli deposit, are characterized by predominantly flat terrain. As a result, the sparse occurrence of topographic structures occurring in these areas was primarily utilized to reinforce observations derived from the magnetic and electromagnetic data.

6.1.2 Magnetic data

Structures with high magnetic susceptibility are found mainly in the northernmost part of the map area and, naturally, in association with the Tapuli and Sahavaara deposits (Figure 26). Still, large portions of the area exhibit a relatively low magnetic signature (depicted in blue and green), indicating an absence or deficiency of highly magnetic minerals in the bedrock. In these areas, very few magnetic lineaments occur, and interpretations were largely based on the topographic and electromagnetic data.

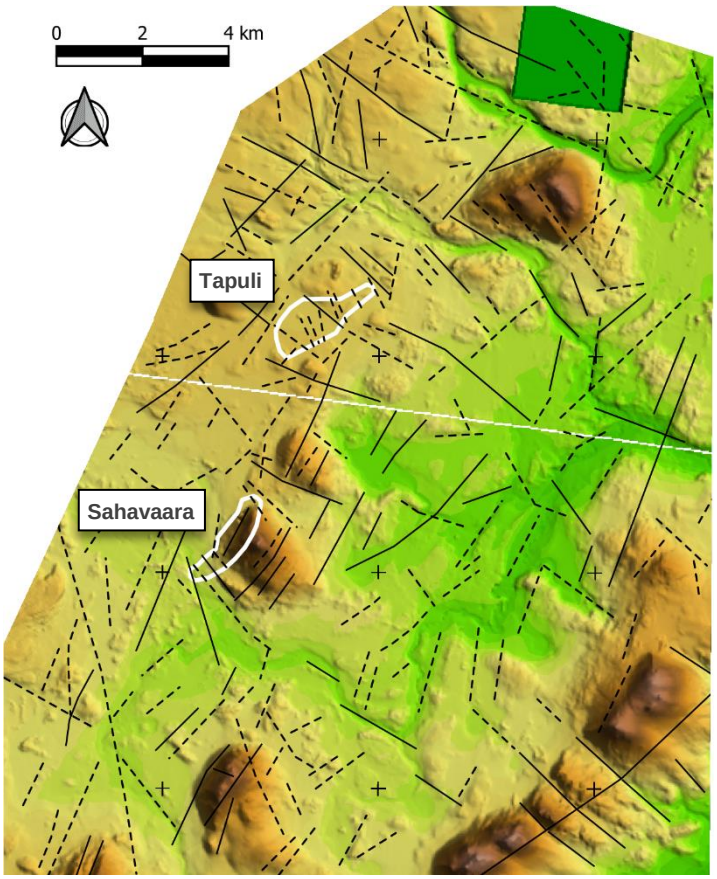

Figure 25. Topographic map of the study area (with shading from northeast) showing all 217 combined lineaments. Three major NW-SE oriented topographic depressions are prominent in the south-eastern map area.

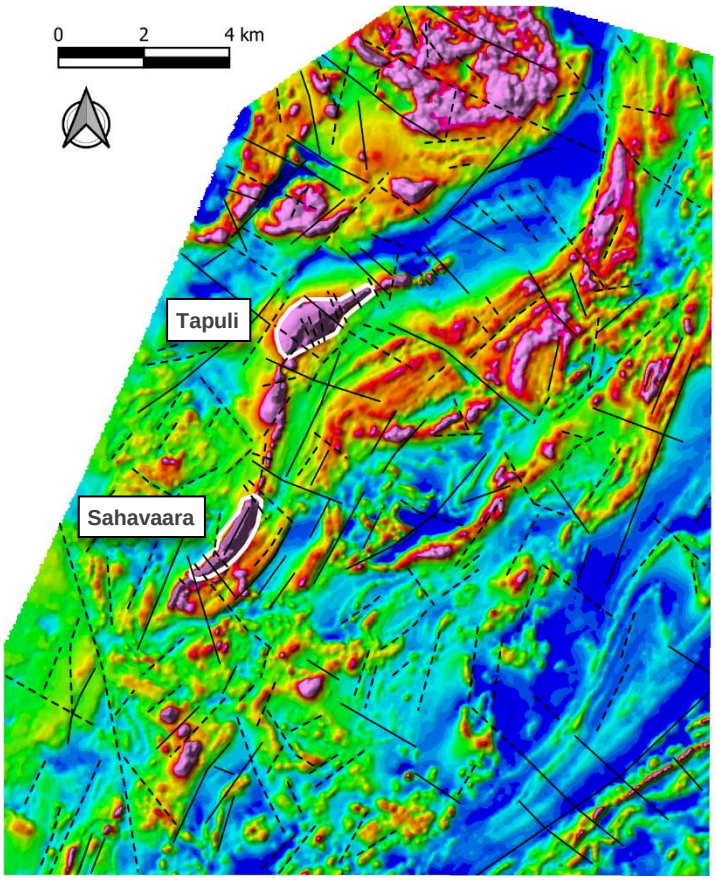

Figure 26. Magnetic map of the study area showing all 217 combined lineaments. The magnetic pattern is dominated by NE-SW to NNE-SSW structures. Banded and curved structures are interpreted to be products of ductile deformation. Magnetic susceptibility is indicated by purple (high susceptibility) to blue (low susceptibility).

Overall, the magnetic pattern is broadly characterized by NE-SW to NNE-SSW oriented structures. Magnetic banding and rounded formations, found mainly in the central and south-eastern parts, are interpreted as products of extensive ductile deformation (folding, shearing, and compositional banding). In the central map area, a major NW-SE oriented low-magnetic anomaly transects the magnetic banding and appears to offset the surrounding geological units with an estimated sinistral displacement of roughly 100 m. Although the lineament corresponding to this structure was considered a confident interpretation based on the apparent displacement, it could not be supported by the other data types or the satellite imagery. However, the structure is situated in a topographically flat area which is largely overlaid by the Tapuli mine tailings pond (Figure 27). As a result, most superficial structures within this area are likely undetectable in both the topographic data and aerial imagery.

A cluster of shorter (500–900 m) NNW-SSE oriented lineaments located within the Tapuli pit area were also interpreted exclusively from the magnetic data (Figure 27). These interpretations could not be reinforced by the other data types, or by any evident displacement, and were thus considered less confident interpretations. The strong magnetic signature of the Tapuli mineralisation, coupled with flat local terrain, presented difficulties in producing confident interpretations. Resultantly, only one confident interpretation (observed in both the magnetic and topographic data) was derived within the pit area: a roughly 1,100 m long, NW-SE oriented lineament that bisects the north-eastern part of Central pit.

To the south, a WNW-ESE oriented lineament, spanning approximately 2,800 m, was interpreted based on observations across all the available data types. In the magnetic data, this lineament appears to displace a minor segment of unmined mineralisation southwest of Tapuli Central pit (Figure 27). While estimating a horizontal displacement of roughly 100 m in dextral movement, the displacement could not be observed in the topographic and electromagnetic data.

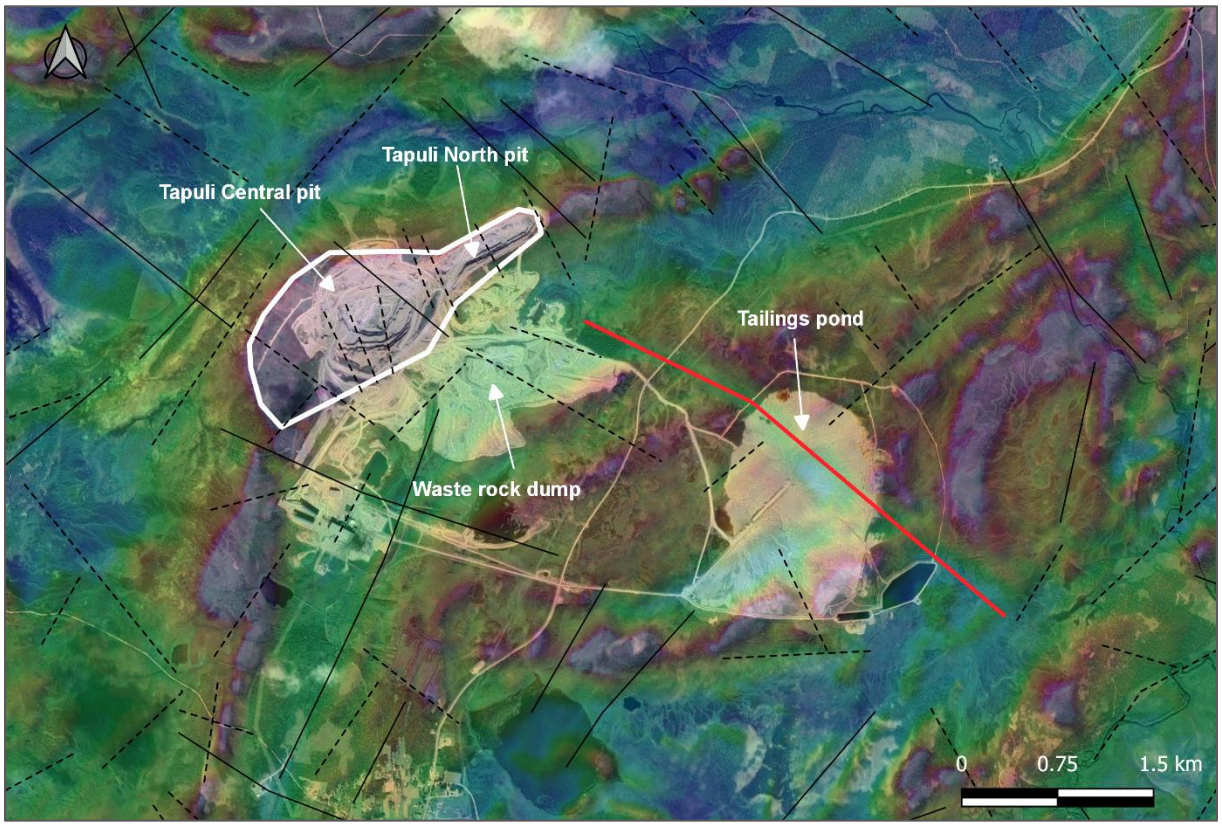

Figure 27. Satellite image of the Tapuli mine area superimposed onto the magnetic map. A major NW-SE oriented low-magnetic anomaly (red line) bisects the tailings pond.

6.1.3 Electromagnetic data

The electromagnetic maps were primarily used to support interpretations derived from the topographic and magnetic data, and to identify possible large-scale groundwater conduits. Emphasis was placed on the higher frequency data (25 kHz) since the lower frequency analogue (0.9 kHz) was considered inadequate in accentuating poorer conductors such as soil, clay alteration, and water-bearing fractures (i.e., features commonly associated with brittle deformation).

The most prominent feature in the 0,9 kHz data is a several kilometres long high-conductive anomaly, oriented NNE-SSW to NE-SW, which extends north-eastwards from the Sahavaara deposit (Figure 28). This anomaly is assumed to correlate with graphite-rich rocks belonging to the Veikkavaara greenstone group (see section 4.1.3 & 4.2.1). To the southwest, a comparable anomaly is bisected by a roughly 8,300 m long NNW-SSE oriented lineament which extends outside the map area. The lineament, which initially was interpreted from the magnetic data, crosscuts the hinge of what appears to be a fold structure in the southwestern graphite-bearing formation. No evident displacement associated with the lineament could be observed in any of the data sets, leading to its classification as a less confident interpretation.

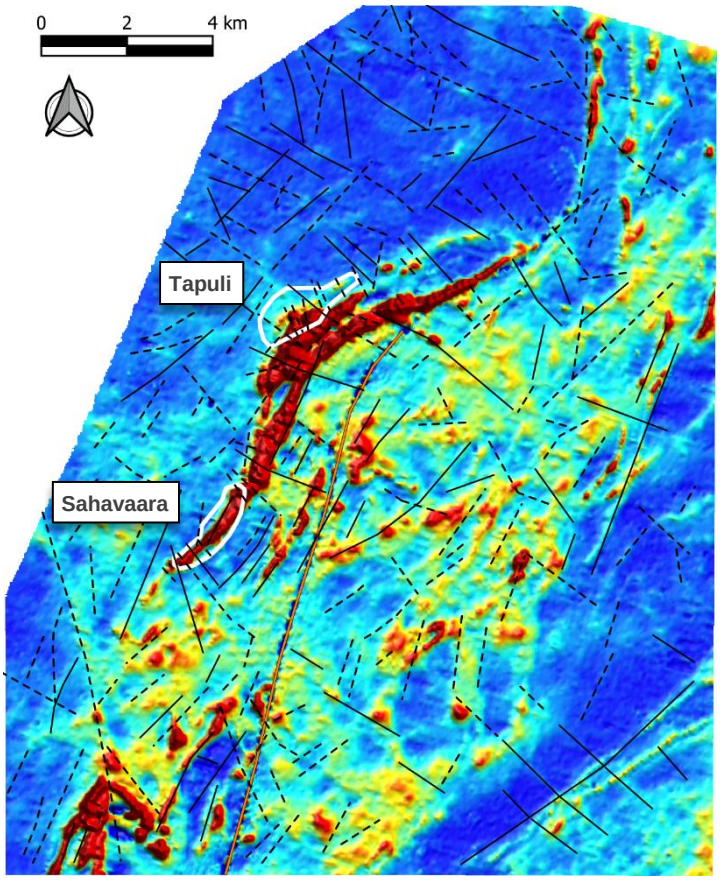

Figure 28. Electrical conductivity map of the study area (0.9 kHz, imaginary component). Pronounced high-conductive anomalies (red) are interpreted as graphite-rich rocks. The orange N-S oriented line indicates the location of a major power line, producing a "false" anomaly.

A total of 60 topographic and magnetic lineaments could be spatially correlated with linear high-conductive anomalies observed in the 25 kHz electromagnetic data (Figure 29). These anomalies were interpreted as water-bearing fractures and occur primarily in areas exhibiting relatively low conductivity. The irregular pattern formed by *non-linear* high-conductive anomalies in the same data is assumed to correspond with superficial deposits such as peat or till. It is therefore important to note that the conductive signature of water-bearing fractures can potentially be indiscernible in the presence of conductive overburden. As a result, the distribution of major water-bearing fractures in the study area is likely more extensive than what's indicated by this interpretation.

A distinctive feature in the 25 kHz data is a 1,200 m long NNE-SSW oriented lineament, interpreted as a major water-bearing fracture, situated within the Sahavaara deposit (Figure 29). Several similarly oriented high-conductive lineaments are also present to the north, east and west of the deposit, suggesting considerable fluid flows in the area. Comparatively, large-scale water-bearing fractures appear to be notably less prevalent in the Tapuli area. Nevertheless, this interpretation is by no means conclusive and could be influenced by a wide range of factors, including local variations in thickness and conductivity of the overburden.

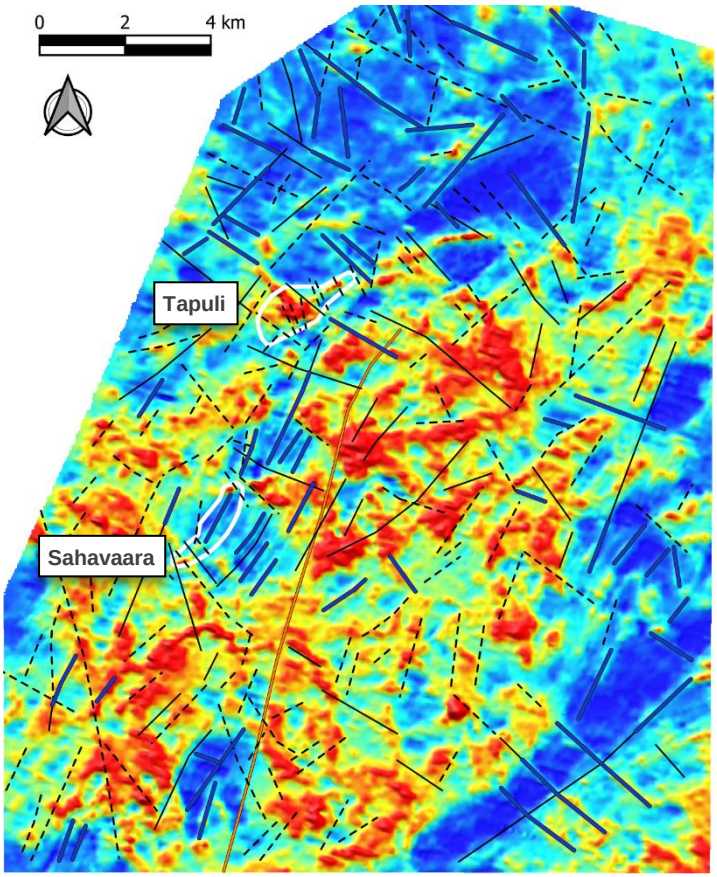

Figure 29. Electrical conductivity map of the study area (25 kHz, imaginary component). Lineaments interpreted as water-bearing fractures are indicated by thick blue lines. Non-linear high-conductive anomalies (red-yellow) is interpreted as superficial deposits.

6.2 Structural analysis

A total of 137 fault planes, derived from the 3D model of Tapuli Central pit, were digitized and measured for strike and dip using the right-hand rule (Figure 30). However, due to certain areas of the pit lacking discernible fault planes or being obscured by loose rock material from recent production blasts, a uniform collection of measurements across the pit was unattainable. Consequently, measurements were predominantly obtained from the eastern pit walls, which accounts for more than half of the total measurements. Furthermore, limitations in the vertical resolution of the 3D model prohibited the collection of measurements from the lowermost benches, as highlighted in section 5.2.

Throughout the analysis, particular attention was directed toward the uppermost benches situated in the northern and western segments of the pit, where sedimentary rocks in the hanging wall are widely exposed. This focused approach aimed to prevent misidentification of bedding planes in the sedimentary rocks as fault planes, given their similar physical characteristics. By emphasizing these areas, the analysis sought to ensure accurate differentiation between fault structures and sedimentary features.

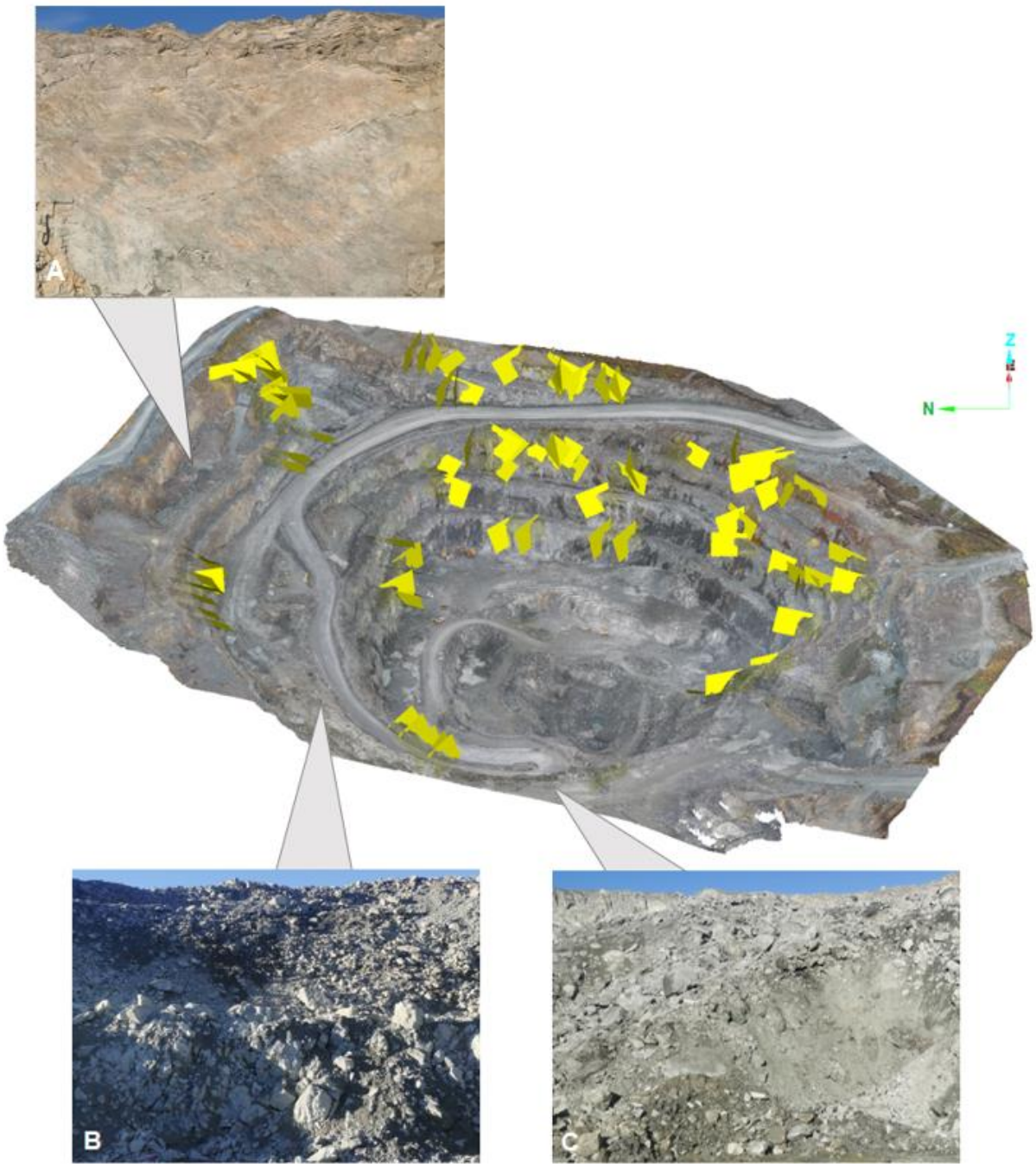

Figure 30. 3D model of Tapuli Central pit. East-facing view showing polygons fitted to exposed fault planes. Several polygons have been removed from this figure to improve the presentation. Measurements could not be collected uniformly as portions of the pit walls lacked distinct fault planes (A) or were covered by rock material (B, C).

6.2.1 Fault plane orientations

Plotting the structural data reveals at least four dominant orientational groups, striking NE, SW, SE, and SSE (Figure 31). Group 1, 2, and 3 are well-developed and constitute roughly 90% of the total measurements. The distribution of the groups within the pit is inconsistent, as group 1 and 2 are found almost exclusively on the northern and eastern pit walls, respectively (Figure 32). In contrast, groups 3 and 4 can be traced across the pit and appear on both sides of opposing pit walls. It is unclear whether this inconsistency is a natural effect or if it results from biased measurements.

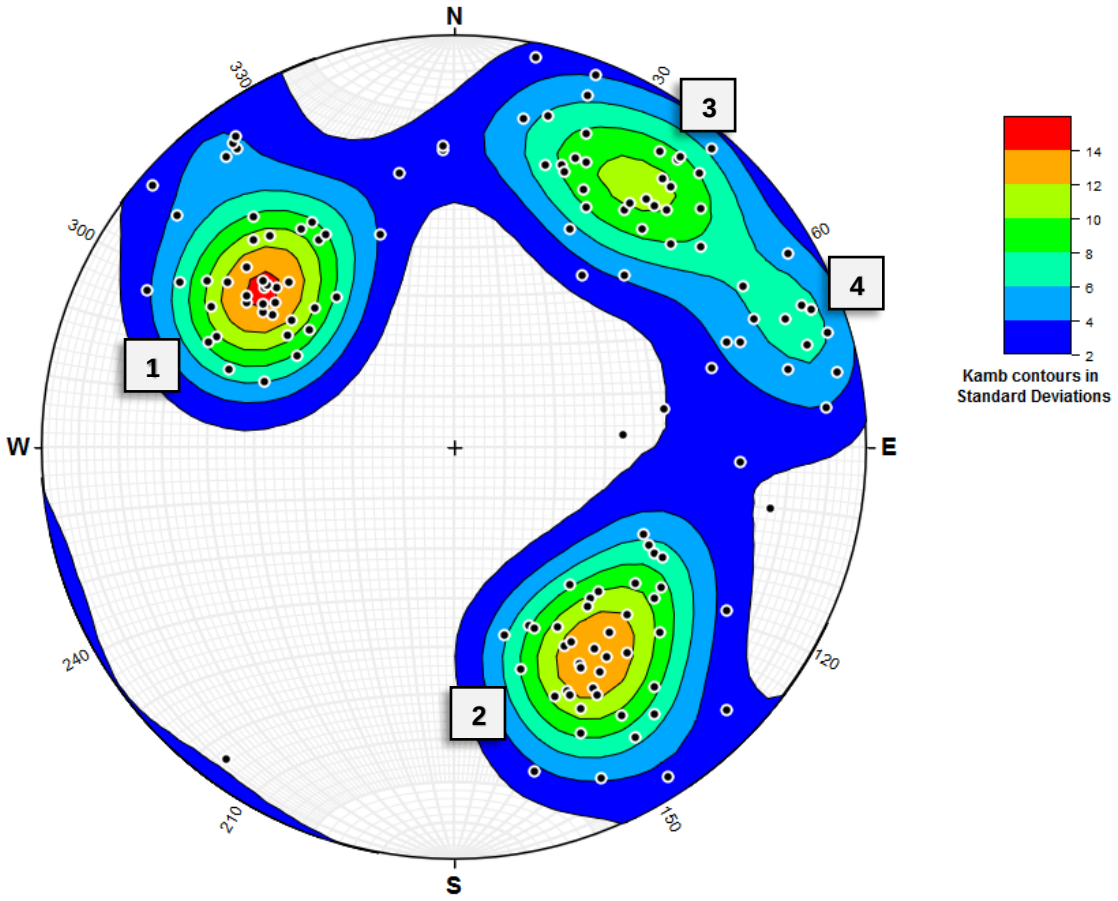

Figure 31. Pole plot of the structural data (n = 137) showing four dominant orientational groups.

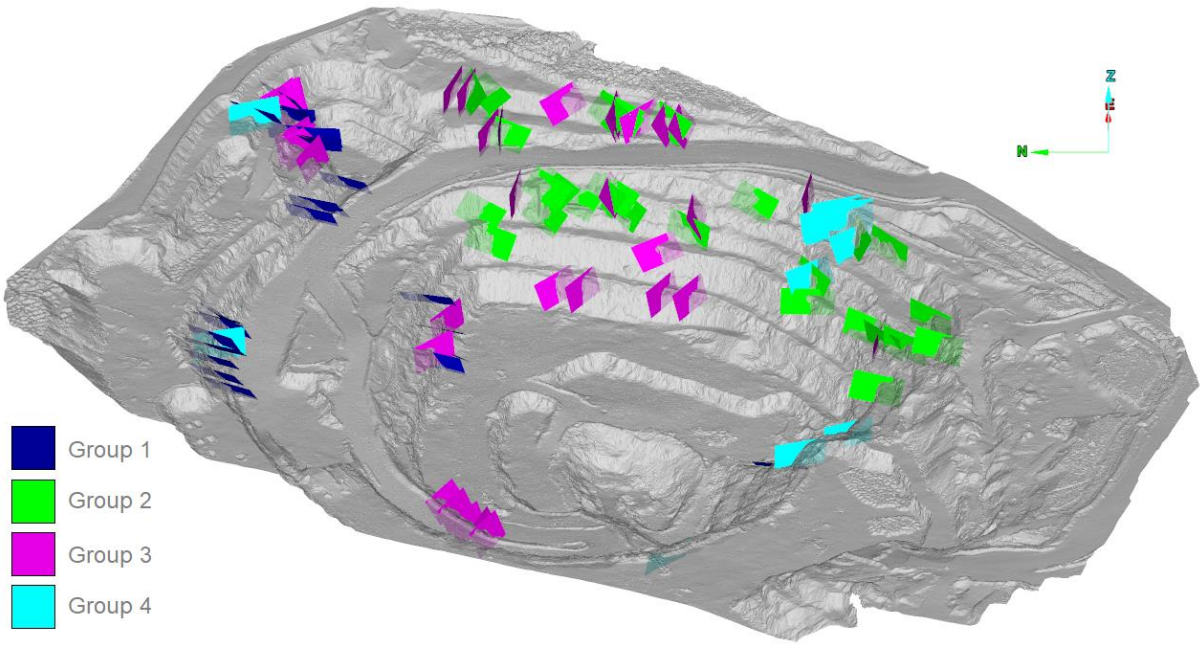

Figure 32. Measured fault planes divided into groups based on strike. Inclined view from the west.

Dip angles typically range from moderate to steep, peaking at around 40–70°, with only three measurements displaying dips less than 30° (Figure 33).

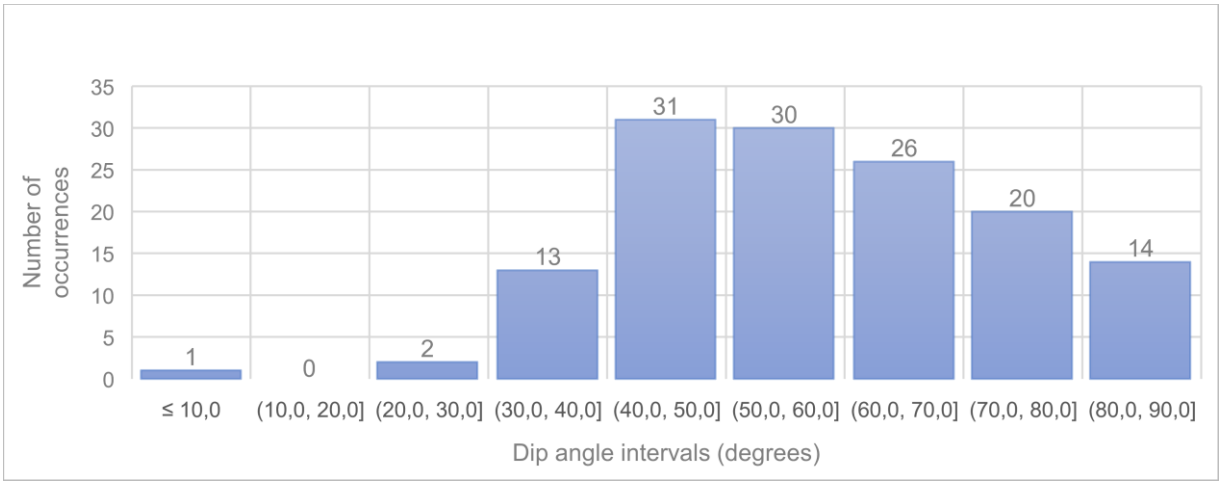

Figure 33. Histogram showing the number of occurrences for measured dip angles divided into fixed 10° intervals.

6.2.2 Field verification

The structural analysis was validated through on-site visual verification within the pit, aimed at confirming interpretations derived from the 3D model and eliminating inaccuracies caused by digital artifacts, bedding planes, or other planar structures. Of the 137 fault planes interpreted, 71 could be confirmed on-site. Unfortunately, the remaining 66 fault planes were situated in inaccessible pit areas and thus could neither be affirmed nor dismissed. Nonetheless, the successful validation of all accessible interpretations suggests the viability of this method.

The confirmed fault planes exhibited geometries consistent with the broader fracture patterns observed on the corresponding pit walls. Only natural fractures were considered, while those induced by blasting (recognized as irregular zones around drill holes) were purposefully excluded. Interestingly, several gently dipping (5–20°) fault planes were observed in the pit. Despite their ample exposure and sufficient size for accurate 3D reproduction, these fault planes were not observed in the 3D model and, hence, not included in the structural measurements. Neither do their geometries align with the general trend of steeply to moderately dipping fault planes observed in the dip data (Figure 33). It is therefore likely that fault planes oriented in such fashion (i.e. gently dipping) are widely overlooked by this approach, since parallel and sub-parallel orientations are unfavourable when utilizing the surface reconstruction method (discussed in section 5.2).

6.3 Summary of results

A comprehensive two-stage analysis of geological features, emphasizing lineaments and structural measurements by employing diverse data types and interpretative methods, was conducted during this project. The lineament analysis yielded 217 interpreted lineaments, showcasing dominant orientations of NW-SE to NNW-SSE and NE-SW to NNE-SSW, as well as indicating substantial fluid flows in the bedrock in the Sahavaara deposit area. Concurrently, the structural analysis, centred on digitizing and measuring fault planes, resulted in 137 structural measurements classified into four main groups striking NE, SW, SE, and SSE, respectively. Notably, the SSE striking group is distinctly less pronounced in the data compared to the other groups.

7 Discussion

7.1 Limitations and errors

Combining topographic and geophysical data in GIS enabled a comprehensive interpretation. However, the accuracy of interpretations is contingent upon the interpreter's subjectivity and knowledge, as well as the data quality, the latter being shaped not only by data collection methods but also by the physical characteristics of the study area or object under investigation. This is exemplified by the difficulties encountered in confidently interpreting lineaments from topographic and magnetic data in regions characterized by flat terrain or significant magnetic mineralization, underscoring the importance of cross-data validation to enhance confidence in geological interpretations. To reinforce interpretation confidence further, integrating a geological map with primary rock units could have served as valuable complementary data.

The method employed for structural measurements in this project presents inherent limitations linked to the 3D modelling process. Although unaffected by mineralization's magnetic properties, this approach faces constraints related to the model's resolution, particularly in capturing fault planes of small dimensions. Furthermore, the surface reconstruction method's accuracy requires photography captured orthogonally to the surface. The use of overhead drone photography resulted in the omission of fault planes with certain geometries from the measurements, diminishing their inclusion in the analysis. Consequently, the method yielded a reduced number of measurements compared to conventional techniques, impacting the study's comprehensiveness and highlighting a methodological gap. It is important to recognize that this methodology exclusively focuses on planar structures (i.e. faults and fault zones) for identifying brittle deformation. This limitation suggests potential oversight of non-planar brittle deformation.

It is also important to point out the distinction between lineaments, which are two-dimensional features (x, y), and structural measurements involving strike and dip data, which capture the orientation of planes in three dimensions (x, y, z). As a result, the correlation between a lineament's and a fault plane's orientations is limited to the strike of the latter and doesn't encompass the dip angle or dip direction.

7.2 Data correlation

Given its focus on brittle deformation in the Tapuli area, the 2009 hydrological study (see section 4.3.2) conducted by Vaittinen et al. (2009) stands as a key reference for potential correlation. The authors discerned four primary orientational groups from extensive fracture logs (Table 3). These included fractures striking SW with steep dips towards the NW, which emerged as the dominant trend, along with fractures striking NE, SE, and NW. Notably, the first three trends are consistent with the structural measurements obtained during this project (Table 4). However, the fourth trend, which strikes NW as per the hydrological study, is practically non-existent in the measurements derived from the 3D model as it was observed in only 1 out of 137 measurements (Figure 31). According to Vaittinen et al. (2009), the NW striking trend is found mainly in the surface portion (<100 m below surface) of the hanging wall. Since the hanging wall is exposed primarily along the western pit walls, which are scarcely represented in the structural analysis, it is likely that this discrepancy stems from these biased measurements.

The absence of NW striking fault planes in the structural measurement does not hamper the consistency regarding the lineament analysis, in which NW-SE oriented lineaments are abundant (Figure 24-29). This particular orientation is de facto widely represented in the structural analysis by the SE-striking faults dipping towards SW (group 3). Furthermore, major NW-SE oriented structures appear at a regional scale, as one of three groups of major discontinuities identified from magnetic and gravity data

by Luth et al. (2001) and Bergman et al. (2018). The other two groups identified by these authors were oriented NNW-SSE and NNE-SSW, which also aligns with the outcome of the lineament analysis.

A geological map of the study area, showing deformation zones identified by The Geological Survey of Sweden (SGU) together with all 217 interpretations from the lineament analysis, is presented in Figure 34. Dominant orientations in the SGU data are roughly NW-SE and NE-SW. Interestingly, two shorter deformation zones, bisecting the Tapuli deposit in an NNW-SSE direction, are orientationally coherent with group 4 in the structural data from Central pit (Figure 31 & 32, Table 4). This orientation is, however, almost absent in Vaittinen et al. (2009) except for a few occurrences observed within the skarn. The reason for inconsistency is unknown.

Table 3. Dominant orientational trends observed in drillholes from the Tapuli area (Vaittinen et al., 2009).

Group	Strike	Dip dir.	Dip angles
1	NE	SE	Gentle-moderate
2	SW	NW	Moderate-steep
3	SE	SW	Steep
4	NW	NE	Steep

Table 4. Dominant orientational trends derived from structural analysis of Tapuli Central pit 3D model.

Group	Strike	Dip dir.	Dip angles
1	NE	SE	Moderate
2	SW	NW	Moderate
3	SE	SW	Moderate-steep
4	SSE	WSW	Moderate-steep

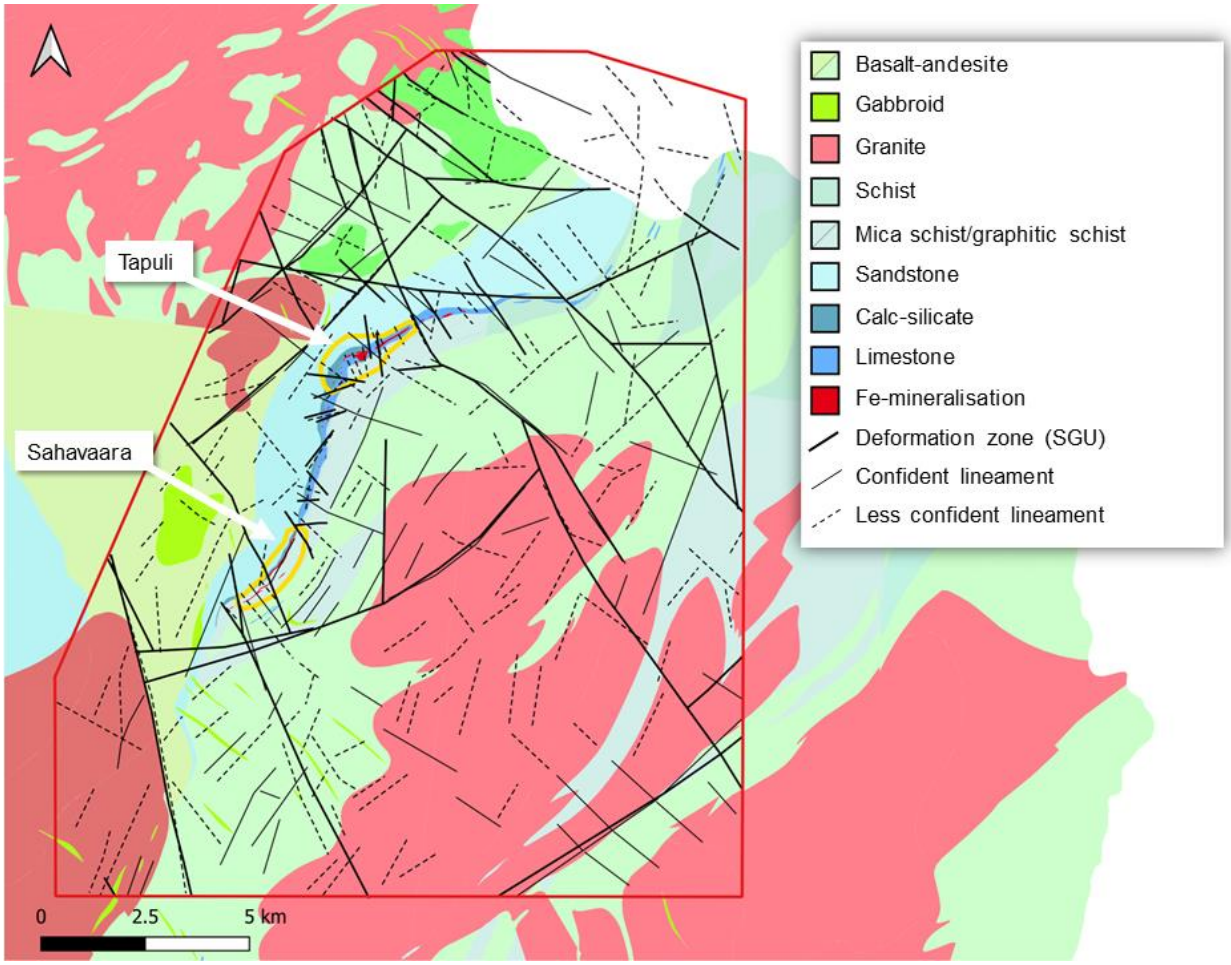

Figure 34. Geological map of the study area showing main rock types and deformation zones (thick black lines) mapped by the Geological Survey of Sweden (SGU), as well as all 217 lineament interpretations (thin black and dotted lines). Locations of the Tapuli and Sahavaara deposits indicated in yellow. Modified from SGU (2020).

8 Conclusions

A structural geological model of the Kaunisvaara mining area, located in Norrbotten county, was established by integrating geophysical and structural geological data. A lineament analysis, encompassing the area surrounding the Tapuli and Sahavaara deposits, was supplemented with a structural analysis of Tapuli central pit.

The outcome of the respective analyses exhibited mostly consistent findings, reinforcing the observed dominant orientations across the geological formations and scales, and aligning well with previous studies conducted at both regional and local levels.

Indicated major fluid flows in the Sahavaara deposit area remains inconclusive. As such, its essential to emphasize the preliminary nature of interpretations based on geophysical data and stress the necessity of field verification for conclusive evidence.

Although a viable method, structural measurements derived from point cloud-generated models have inherent constraints when applied to brittle deformation in an open pit setting.

9 Acknowledgments

I want to thank my supervisor Professor Ulf Söderlund for all his engagement and support. I also want to thank Håkan Mattsson and Hans Thunehed for all their help regarding the lineament analysis.

10 References

Aker Solutions. (2010). Executive Summary. Kaunisvaara Feasibility Study. Report prepared for Northland Resources AB. Aker Solutions ASA. October 2010.

Baker, H. & Bonson, C. (2013). Evaluation of the Structural Geology of the Tapuli Iron Ore Project, Norrbotten, Sweden. Report UK5334 prepared for Northland Resources AB. SRK (UK) Limited.

Baker, H., Pattinson, D. & Reardon, C. (2011). Technical Review of the Kaunisvaara Iron Project, Sweden, June 2011. Report U4067 prepared for Northland Resources AB. SRK (UK) Limited.

Bergman, S., Kübler, L. & Martinsson, O. (2001). Description of Regional Geological and Geophysical Maps of Northern Norrbotten County (East of Caledonian Orogen). Report BA56. SGU.

Bergman, S., Billström, K., Persson, P.-O., Skiöld, T. & Evins, P. (2006). U-Pb age evidence for repeated Palaeoproterozoic metamorphism and deformation near the Pajala shear zone in the northern Fennoscandian shield. GFF 128, 7–20.

Bergman, T. & Hellström, F. (2020). Inventory of Mineral Resources in Northeastern Norrbotten County, Sweden. Report 2020:09. SGU.

Degnan, J., Moore, R., & Mack, T.J. (2001). Geophysical investigations of well fields to characterize fractured-bedrock aquifers in southern New Hampshire. Water-Resources Investigations Report.

Denisova, N. (2013). Sulfide Distribution and its Relation to Different Types of Skarn Alteration at the Tapuli Deposit, Northern Sweden. Master's thesis. Luleå Tekniska Universitet. Obtained from: http://www.diva-portal.org/smash/record.jsf?pid=diva2%3A1027996&dswid=2237.

Dishaw, G. & Lepley, B. (2021). A Mineral Resource Update for the Tapuli Iron Ore Deposit, Sweden. Report 31107 prepared for Kaunis Iron. SRK (UK) Limited.

Eriksson, B. & Hallgren, U. (1975). Beskrivning till berggrundskartbladen Vittangi NV, NO, SV, SO. Sveriges geologiska undersökning Af 13–16, 203.

Grigull, S., Berggren, R., Jönberger, J., Jönsson, C., Hellström, F.A. & Luth, S. (2018). Folding observed in Palaeoproterozoic supracrustal rocks in northern Sweden. In: Bergman, S. (ed.): Geology of the Northern Norrbotten ore province, northern Sweden. Sveriges geologiska undersökning, Rapporter och meddelanden 141, 205–255.

Guo, B., Wang, J., Jiang, X., Li, C, Su, B., Cui, Z., Sun, Y., & Yang, C.L. (2020). A 3D Surface Reconstruction Method for Large-Scale Point Cloud Data. Mathematical Problems in Engineering, vol 2020, Article ID 8670151. https://doi.org/10.1155/2020/8670151.

Hellström, F. & Bergman, S. (2016). Is there a 1.85 Ga magmatic event in northern Norrbotten? − U-Pb SIMS zircon dating of the Pingisvaara metagranodiorite and the Jyryjoki granite, northern Sweden, GFF, doi: 10.1080/11035897.2016.1171254.

Hellström, F.A. (2018). Early Svecokarelian migmatisation west of the Pajala Deformation Belt, northeastern Norrbotten Province, northern Sweden. In: Bergman, S. (ed): Geology of the Northern Norrbotten ore province, northern Sweden. Rapporter och Meddelanden 141, Sveriges geologiska undersökning. 361–379.

Helmenstine, A.M. (2020). August 27: Table of Electrical Resistivity and Conductivity. Retrieved from https://www.thoughtco.com/table-of-electrical-resistivity-conductivity-608499, September 17, 2021.

Henkel, H. & Guzmán, M. (1977). Magnetic features of fracture zones. Geoexploration, Vol. 15, No. 3, 173–181.

Karato, S.I.& Wang, D. (2013). Electrical Conductivity of Minerals and Rocks. Physics and Chemistry of the Deep Earth. Wiley-Blackwell. March 24th, 2013. 145–182.

Lahtinen, R., Huhma, H., Lahaye, Y., Jonsson, E., Manninen, T., Lauri, L.S., Bergman, S., Hellström, F., Niiranen, T. & Nironen, M. (2015). New Geochronological and Sm-Nd Constraints Across the Pajala Shear Zone of Northern Fennoscandia: Reactivation of a Paleoproterozoic Suture. Precambrian Research 256, 102–119.

Lindholm, T. (2009). Pellivuoma Resource Estimate. Report GVR09020 prepared for Northland Exploration. GeoVista. Obtained from: www.sedar.com.

Lindroos, H., Nylund, B. & Johansson, K. (1972). Tapuli och Palotieva järnmalmsfyndigheter. Rapport rörande resultaten av SGU:s undersökningar under åren 1963–1969. Report 68:2. SGU.

Luth, S., Jönsson, C., Jönberger, J., Grigull, S., Berggren, R., Van Assema, B., Smoor, W. & Djuly, T. (2018). The Pajala Deformation Belt in northeast Sweden: Structural geological mapping and 3D modelling around Pajala. In: Bergman, S. (ed.): Geology of the Northern Norrbotten ore province, northern Sweden. Sveriges geologiska undersökning, Rapporter och Meddelanden 141, 259–285.

Lynch, E.P., Bauer, T.E., Jönberger, J., Sarlus, Z., Morris, G. & Persson, P.-O. (2018). Petrological and structural character of c. 1.88 Ga meta-volcanosedimentary rocks hosting iron oxide-copper-gold and related mineralisation in the Nautanen–Aitik area, northern Sweden. In: Bergman, S. (ed.): Geology of the Northern Norrbotten ore province, northern Sweden. Sveriges geologiska undersökning Rapporter och Meddelanden 141, 107–149.

Martinsson O. (1997). Paleoproterozoic greenstones at Kiruna in northern Sweden: a product of continental rifting and associated mafic-ultramafic volcanism. In O. Martinsson: Tectonic setting and metallogeny of the Kiruna greenstones. Doctoral thesis 1997:19, Paper I, 1–49. Luleå University of Technology.

Martinsson, O., Bergman, S., Persson, P.-O., Schöberg, H., Billström, K. & Shumlyanskyy, L. (2018). Stratigraphy and ages of Palaeoproterozoic metavolcanic and metasedimentary rocks at Käymäjärvi, northern Sweden. In: Bergman, S. (ed.): Geology of the Northern Norrbotten ore province, northern Sweden. Sveriges geologiska undersökning Rapporter och Meddelanden 141, 79–105.

Martinsson, O. (2004). Geology and metallogeny of the northern Norrbotten Fe-CU-Au Province. Society of Economic Geologists Guidebook Series 33, 131-148.

Martinsson, O., Billström, K., Broman, C., Weihed, P., Wanhainen, C. (2016). Metallogeny of the Northern Norrbotten Ore Province, northern Fennoscandian Shield with emphasis on IOCG and apatite-iron ore deposits. Ore Geology Reviews (2016). Doi: 10.1016/j.oregeorev.2016.02.011

Martinsson, O. & Perdahl, J.A. (1995). Paleoproterozoic extensional and compressional magmatism in northern Sweden. Svecofennian volcanism in northern Sweden, Doctoral thesis 1995:169D, Paper II. Luleå University of Technology. 1-13.

Martinsson, O., Vaasjoki, M. & Persson, P.-O. (1999). U-Pb ages of Archaean to Palaeoproterozoic granitoids in the Torneträsk-Råstojaure area, northern Sweden. In S. Bergman (ed.): Radiometric dating results 4. Sveriges geologiska undersökning C 831, 70–90.

Moilanen, M. & Peltonen, P. (2015). The Hannukainen Fe-(CU-Au) Deposit, Western Finnish Lapland. Mineral Deposits of Finland, 485–505.

Niiranen, T., Poutiainen, M. & Mänttäri, I. (2007). Geology, geochemistry, fluid inclusion characteristics, and U-Pb age studies on iron oxide-Cu-Au deposits in the Kolari region, northern Finland. Ore Geology Reviews 30, 75-105.

Niiranen, T. (2005). Iron-Oxide-Copper-Gold Deposits in Finland. Academic dissertation. Faculty of Science of the University of Helsinki.

Niiranen, T. (2011). IOCG and Porphyry-Cu deposits in northern Finland and Sweden. Excursion guide, 25th International Applied Geochemistry Symposium 22-26 August Rovaniemi, Finland.

Nironen, M. (1997). The Svecofennian Orogen: A tectonic Model. Precambrian Research 86, 21-44.

O´Leary, D.W., and Friedman, J. D. (1978). Towards a workable lineament symbology. Proceedings of the third international Conference on the new basement tectonics, Basement Tectonics Committee Publication #3, Basement Tectonic Committee, Inc., Denver, Colorado, 29-31.

Palmén, J., Ahokas, H., Nummela, J. & Saksa, P. (2009). Hydrological data review and preliminary assessment of hydrological bedrock conditions in Tapuli. Hydrology Study, Phase 1. Report 67080612.BGF01. Pöyry Environment Oy, Vantaa.

Perman, F., Bertilsson, R., Tornéus, L. & Andersson, C. (2009). Geotechnical Pit Slope Stability Analysis for the Tapuli Open Pit Mine – Phase 3: Data Collecting and Testing. Report 2769800_03. Vattenfall AB.

Romer, R.L., Martinsson, O. & Perdahl, J.-A. (1994). Geochronology of the Kiruna iron ores and hydrothermal alterations. Economic Geology 89, 1249–1261.

Romer, R.L. (1996). What is the significance of lead isotope data from stilbite, a low-temperature natural ion-exchanger? The 22nd Nordic Geological Winter meeting, Turku, Åbo, Abstracts, 172.

Saksa, P., Eloranta, T., Nummela, J., Tuomela, P. & Sallinen, P. (2009). Tapuli Hydrological Investigations. Field Investigations and Data, Phase 3. Report 67090063.BGF. Pöyry Environment Oy, Vantaa.

Vaittinen, T., Karvonen, T., Saksa, P., Eloranta, T., Nummela, J., Heikkinen, J., Palmén, J. & Ahokas, H. (2009). Tapuli Hydrological Investigations. Groundwater flow analysis and modelling, phase 4. Report 67090063.BGF2. Pöyry Environment Oy, Vantaa,

Wright, S.F. (1988). Early Proterozoic deformational history of the Kiruna district, northern Sweden. Unpublished Doctoral thesis, University of Minnesota, 170.

Tidigare skrifter i serien ”Examensarbeten i Geologi vid Lunds universitet”:

622. Selezeneva, Natalia, 2021: Indications for solar storms during the Last Glacial Maximum in the NGRIP ice core. (45 hp)
623. Bakker, Aron, 2021: Geological characterisation of geophysical lineaments as part of the expanded site descriptive model around the planned repository site for high-level nuclear waste, Forsmark, Sweden. (45 hp)
624. Sundberg, Oskar, 2021: Jordlagerföljden i Höjeådalen utifrån nya borrningar. (15 hp)
625. Sartell, Anna, 2021: The igneous complex of Ekmanfjorden, Svalbard: an integrated field, petrological and geochemical study. (45 hp)
626. Juliusson, Oscar, 2021: Implications of ice-bedrock dynamics at Ullstorp, Scania, southern Sweden. (45 hp)
627. Eng, Simon, 2021: Rödslam i svenska kraftdammar - Problematik och potentiella lösningar. (15 hp)
628. Kervall, Hanna, 2021: Feasibility of Enhanced Geothermal Systems in the Precambrian crystalline basement in SW Scania, Sweden. (45 hp)
629. Smith, Thomas, 2022: Assessing the relationship between hypoxia and life on Earth, and implications for the search for habitable exoplanets. (45 hp)
630. Neumann, Daniel, 2022: En mosasaurie (Reptilia, Mosasauridae) av paleocensk ålder? (15 hp)
631. Svensson, David, 2022: Geofysisk och geologisk tolkning av kritskollors utbredning i Ystadsområdet. (15 hp)
632. Allison, Edward, 2022: Avsättning av Black Carbon i sediment från Odensjön, södra Sverige. (15 hp)
633. Jirdén, Elin, 2022: OSL dating of the Mesolithic site Nilsvikdalen 7, Bjorøy, Norway. (45 hp)
634. Wong, Danny, 2022: GIS-analys av effekten vid stormflod/havsnivåhöjning, Morupstrakten, Halland. (15 hp)
635. Lycke, Björn, 2022: Mikroplast i vattenavsatta sediment. (15 hp)
636. Schönherr, Lara, 2022: Grön fältspat i Varbergskomplexet. (15 hp)
637. Funck, Pontus, 2022: Granens ankomst och etablering i Skandinavien under postglacial tid. (15 hp)
638. Brotzen, Olga M., 2022: Geologiska besöksmål och geoparker som plattform för popularisering av geovetenskap. (15 hp)
639. Lodi, Giulia, 2022: A study of carbon, nitrogen, and biogenic silica concentrations in *Cyperus papyrus*, the sedge dominating the permanent swamp of the Okavango Delta, Botswana, Africa. (45 hp)
640. Nilsson, Sebastian, 2022: PFAS- En sammanfattning av ny forskning, med ett fokus på föroreningskällor, provtagning, analysmetoder och saneringsmetoder. (15 hp)
641. Jägfeldt, Hans, 2022: Molnens påverkan på jordens strålningsbalans och klimatsystem. (15 hp)
642. Sundberg, Melissa, 2022: Paleontologiska egenskaper och syreisotopsutveckling i borrkärnan Limhamn-2018: Kopplingar till klimatförändringar under yngre krita. (15 hp)
643. Bjermo, Tim, 2022: A re-investigation of hummocky moraine formed from ice sheet decay using geomorphological and sedimentological evidence in the Vomb area, southern Sweden. (45 hp)
644. Halvarsson, Ellinor, 2022: Structural investigation of ductile deformations across the Frontal Wedge south of Lake Vättern, southern Sweden. (45 hp)
645. Brakebusch, Linus, 2022: Record of the end-Triassic mass extinction in shallow marine carbonates: the Lorüns section (Austria). (45 hp)
646. Wahlquist, Per, 2023: Stratigraphy and palaeoenvironment of the early Jurassic volcaniclastic strata at Djupadalsmölla, central Skåne, Sweden. (45 hp)
647. Gebremedhin, G. Gebreselassie, 2023: U-Pb geochronology of brittle deformation using LA-ICP-MS imaging on calcite veins. (45 hp)
648. Mroczek, Robert, 2023: Petrography of impactites from the Dellen impact structure, Sweden. (45 hp)
649. Gunnarsson, Niklas, 2023: Upper Ordovician stratigraphy of the Stora Sutarve core (Gotland, Sweden) and an assessment of the Hirnantian Isotope Carbon Excursion (HICE) in high-resolution. (45 hp)
650. Cordes, Beatrix, 2023: Vilken ny kunskap ger aDNA-analyser om vegetationsutvecklingen i Nordeuropa under och efter Weichsel-istiden? (15 hp)
651. Bonnevier Wallstedt, Ida, 2023: Palaeocolour, skin anatomy and taphonomy of a soft-tissue ichthyosaur (Reptilia, Ichthyopterygia) from the Toarcian (Lower Jurassic) of Luxembourg. (45 hp)
652. Kryffin, Isidora, 2023: Exceptionally preserved fish eyes from the Eocene Fur Formation of Denmark – implications for palaeobiology, palaeoecology and taphonomy. (45 hp)
653. Andersson, Jacob, 2023: Nedslagskratrars

inverkan på Mars yt-datering. En undersökning av Mars främsta ytdateringsmetod ”Crater Counting". (15 hp)

654. Sundberg, Melissa, 2023: A study in ink – the morphology, taphonomy and phylogeny of squid-like cephalopods from the Jurassic Posidonia Shale of Germany and the first record of a loligosepiid gill. (45 hp)
655. Häggblom, Joanna, 2023: En patologisk sjölilja från silur på Gotland, Sverige. (15 hp)
656. Bergström, Tim, 2023: Hur gammal är jordens inre kärna? (15 hp)
657. Bollmark, Viveka, 2023: Ca isotope, oceanic anoxic events and the calcareous nannoplankton. (15 hp)
658. Madsen, Ariella, 2023: Polycykliska aromatiska kolväten i Hanöbuktens kustnära sediment - En sedimentologisk undersökning av vikar i närhet av pappersbruk. (15 hp)
659. Wangritthikraikul, Kannika, 2023: Holocene Environmental History of Warming Land, Northern Greenland: a study based on lake sediments. (45 hp)
660. Kurop, Anna, 2023: Reconstruction of the glacier dynamics and Holocene chronology of retreat of Helagsglaciären in Central Sweden. (45 hp)
661. Frisendahl, Kajsa, 2023: Holocene environmental history of Washington Land, NW Greenland: a study based on lake sediments. (45 hp)
662. Ryan, Cathal, 2023: Luminescence dating of the late Quaternary loess-palaeosol sequence at Velika Vrbica, Serbia. (45 hp)
663. Lindow, Wilma, 2023: U-Pb datering av zirkon i metasediment tillhörande Stora Le-Marstrand, SV Sverige. (15 hp)
664. Bengtsson, Kaisa, 2023: Geologisk karaktärisering av den kambriska Faluddensandstenen i Östersjön och dess lämplighet för koldioxidlagring. (15 hp)
665. Granbom, Johanna, 2023: Insights into simple crater formation: The Hummeln impact structure (Småland, Sweden). (45 hp)
666. Jonsson, Axel, 2023: Datering av vulkanen Rangitoto, Nya Zeeland, genom paleomagnetiska analysmetoder. (15 hp)
667. Muller, Elsa, 2023: Response of foraminifera *Ammonia confertitesta* (T6) to ocean acidification, warming, and Deoxygenation An experimental approach. (45 hp)
668. Struzynska, Patrycja, 2023: Petrography, geochemistry, and origin of deep magmatic cumulates in the Canary Islands – the xenolith record. (45 hp)
669. Krätzer, Tobias, 2023: Artificiella torskrev i Hanöbukten: Förstudie. (15 hp)
670. Khorshidian, Farid, 2023: 3D modelling and resistivity measurements for hydrogeological assessments in the northern part of Vombsänkan. (45 hp)
671. Sundberg, Oskar, 2023: Methodology for Stored Heat “Heat In Place” (HIP) assessment of geothermal aquifers – Exemplified by a study of the Arnager Greensand in SW Scania. (45 hp)
672. Haraldsson, Emil, 2023: Kan akademin hjälpa industrin utveckla mer robusta grundvattenmodeller? En studie av moderna Svenska industriframtagna grundvattenmodeller. (15 hp)
673. Barabas, Ricky, 2024: Kan chockmetamorfos i okonventionella mineral hjälpa till att identifiera nedslagskratrar? (15 hp)
674. Nilsson, Sebastian, 2024: The glaciotectonic evolution of Ven, Sweden: insights from a comprehensive structural, sedimentological, and geomorphological analysis. (45 hp)
675. Brotzen, Olga M., 2024: A new Lagerstätte-like fossil assemblage from the early Silurian of Mösseberg, Sweden. (45 hp)
676. Eng, Simon, 2024: Precursors to the South Atlantic Anomaly - Magnetic field variations in Lake Eilandvlei, South Africa. (45 hp)
677. Husén, Simon, 2024: Structural Geological Model of the Kaunisvaara Mining District, Norrbotten, Sweden. (45 hp)

LUNDS UNIVERSITET

Geologiska institutionen
Lunds universitet
Sölvegatan 12, 223 62 Lund